MICROCOPY RESOLUTION TEST CHART
NATIONAL BUREAU OF STANDARDS-1963-A

S D

NATURAL FREQUENCIES AND MODE

SHAPES OF CURVED RECTANGULAR COMPOSITE

PANELS WITH INTERIOR CUTOUTS

THESIS

AFIT/GAE/AA/85D-16

Richard A. Walley
Capt.   USAF

DEPARTMENT OF THE AIR FORCE

AIR UNIVERSITY

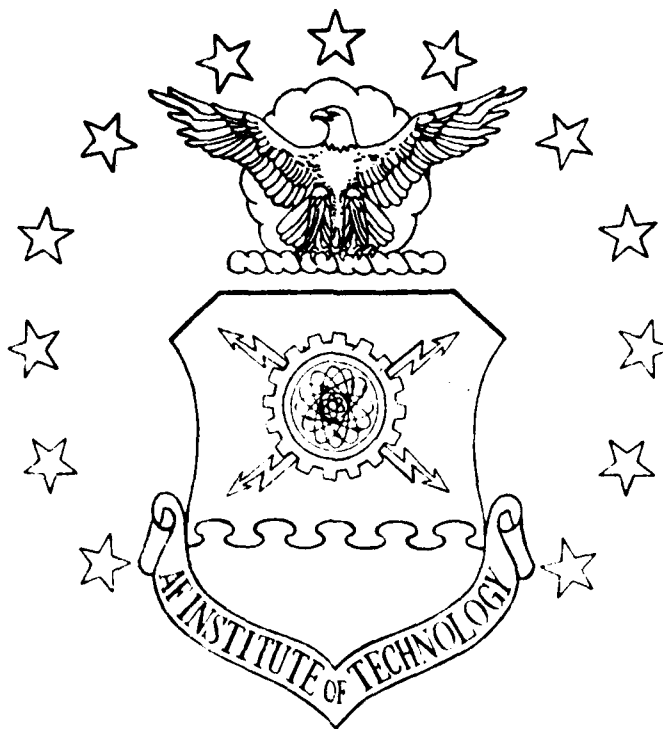# AIR FORCE INSTITUTE OF TECHNOLOGY

Wright-Patterson Air Force Base, Ohio

86 2 12 068

NATURAL FREQUENCIES AND MODE

SHAPES OF CURVED RECTANGULAR COMPOSITE

PANELS WITH INTERIOR CUTOUTS

THESIS

Richard A. Walley
AFIT/GAE/AA/85D-16   Capt.   USAF

AFIT/GAE/AA/85D-16

NATURAL FREQUENCIES AND MODE SHAPES OF CURVED RECTANGULAR

COMPOSITE PANELS WITH INTERIOR CUTOUTS

THESIS

Presented to the Faculty of the School of Engineering

of the Air Force Institute of Technology

Air University

In Partial Fulfillment of the

Requirements for the Degree of

Master of Science in Aeronautical Engineering

Richard A. Walley, B.S.

Captain, USAF

December 1985

ACKNOWLEDGEMENTS

I wish to express my sincere gratitude to Dr. R. L. Hinrichsen for the sharing of his time and the guidance he gave during the course of this study. I also wish to thank Dr. W. L. Mindle and Mr. Gene Maddux for their assistance with the holography. The machinists at the AFIT Model Shop deserve my thanks for their efforts in machining the complex test fixture.

Most of all, I wish to thank my wife, Emma, for her administrative help and support without which I could not have completed this research.

Table of Contents

LIST OF FIGURES

List of Tables

AFIT/GAE/AA/85D-16

ABSTRACT

A finite element computer code, STAGS C-1 and
holographic interferometry were used to determine the
effects of interior cutouts (2 x 2, 2 x 4, and 4 x 4 inch)
on the first five natural frequencies and mode shapes of
curved Graphite Epoxy panels. The panels are a quasi-
isotropic layup $[0, -45, 45, 90]_s$ with a 12 inch chord and
height. Both the finite element and holographic analysis
were conducted using clamped-clamped boundary conditions.

The vibration branch of STAGS C-1 is an energy
technique based on small displacements and linear elastic
stress-strain relationships. When compared with the time
averaged holograms of the experimentally determined natural
frequencies and mode shapes, the two techniques show a close
correlation of both frequency and shape.

It was found that for the 2 x 2 inch cutout, the mode
shapes change very little while the natural frequencies
displayed a small decrease for the higher modes. The 2 x 4
inch cutout retained the general mode shape of the solid
panel for the first two modes. The third through the fifth

modes shapes were changed by this cutout and the loss of

panel stiffness was visible . The 4 × 4 inch cutout exhibit

both a switch in symmetry of the first two modes and a

general decrease in natural frequencies.

ix

I.   INTRODUCTION

Background

Composite materials are used frequently as both primary and secondary structural elements in the construction of modern aircraft. This trend will probably accelerate as the higher performance levels demanded in military aircraft and the increased economy sought by civilian aviation can be achieved through extensive use of these high strength, lightweight materials. In order to use composite materials more extensively in the aircraft industry, a complete understanding of dynamic response is indicated. Curved shells with rectangular cutouts were chosen because this shape is often found in aerospace structures and no closed form solution currently exists. Various studies of a similiar type have been conducted on flat plates. Ashton and Whitney [9] were able to form a solution for symmetric orthotropic plates where no coupling existed between extension and bending. Similiarly, Raju [10] was able to derive exact solutions for circular isotropic plates with central circular holes. Jones and Morgan [11] were able to derive exact numerical solutions for buckling and vibration problems for antisymmetric cross ply shells. Their results

1

show that the effect of coupling between bending and extension on buckling loads and vibration frequencies dies out rapidly as the number of layers increases. However, for unsymmetric shells the coupling dies out very slowly. And in a similiar study, Monahan [12] applied a finite element solution to isotropic rectangular plates with arbitrary cutouts in order to determine their natural frequencies and mode shapes. Results were compared with the results of an holographic analysis.

The logical extension of these efforts was to extend the analysis to a more complex structure and shape. By choosing curved panels with their frequent use in the aerospace field, it is hoped that a valuable contribution can be made to the technology base of composite materials. Additionally, a preliminary evaluation of the STAGS C1 Finite Element Code in modelling real panels is desired.

APPROACH

A parallel effort to utilizing the Finite Element Method (FEM) and laser holography was undertaken to determine the first five natural frequencies and mode shapes of graphite epoxy shells with various retangular cutouts.

The STAGS-Cl computer code developed by B. O. Almroth, F. A. Brogan, and G. M. Stanley of the Lockheed Palo Alto Research Laboratory was chosen due to its ease of application to orthotropic shells and user friendliness. Highly accurate time averaged holography was used to experimentally determine the natural frequencies and mode shapes. An outstanding characteristic inherent to this technique is that its data output is a photographic image readily compared with the contour plots generated from FEM calculations. The natural frequencies and modes shapes extracted by the two methods were compared in order to analyze the effectiveness of the FEM to predict the experimental results.

II. Theory

Finite Elements

The governing equation of motion for a body experiencing free vibration is derived from Newton's Second Law

$$F_E(t) - F_S(t) - F_C(t) = M\ddot{x}(t) \qquad (1)$$

where:

$$\ddot{x}(t) = \text{acceleration}$$
$$F_E(t) = \text{external force}$$
$$F_S(t) = \text{internal elastic forces}$$
$$F_C(t) = \text{damping forces}$$
$$M = \text{mass}$$

The internal damping and elastic forces can be expressed in terms of displacement derivatives and material constants.

$$F_E(t) - Kx(t) - C\dot{x}(t) = M\ddot{x}(t) \qquad (2)$$

where: k = elastic constant   c = damping

By definition a free vibrating body is absent of external forces. In addition, the energy loss mechanism for dry

4

friction and hysteresis losses is not well understood and as is often done with high stiffness low mass structures the structural damping was neglected in this analysis. Assuming displacements are harmonic, equation (2) becomes the fundamental statement of the vibration problem.

$$\{K-\omega^2 M\}D = 0 \qquad (3)$$

where:

ω = circular frequency (rad/sec)

D = displacement vector

The essence of the FEM is the redefinition of a continuous structure in terms of displacements at discrete points or nodes. The STAGS-C1 code is an energy based code using the Kirchoff-Love hypothesis [1]. For a conservative system in equilibrium the total potential energy must be stationary and the first variation will equal zero. The total potential energy of a body is the strain energy of the body minus the work done on the body by external forces. Thus, the total potential energy for a free vibrating body is:

$$\Pi = U$$

$$\text{where } U = 1/2 \int_{volume} (\sigma_x \varepsilon_x + \sigma_y \varepsilon_y + \tau_{xy} \gamma_{xy}) dVol \qquad (4)$$

5

The kinematic relations in STAGS are based on Sander's shell equations [1] expressing total strain as a linear variation of extensional (membrane) and bending (curvature) strains at the midsurface. The midsurface curvatures being composed of components of rotation about coordinate lines and the surface normal.

The midsurface strains are [2]:

$$\varepsilon_x^0 = U_{,x} + 1/2\ \phi_x^2 + 1/2\ \phi^2 \tag{5}$$

$$\varepsilon_y^0 = V_{,y} + W/R + 1/2\ \phi_y^2 - 1/2\ \phi^2 \tag{6}$$

$$2\varepsilon_{xy}^0 = V_{,x} + U_{,y} + \phi_x\phi_y \tag{7}$$

where: ϕ_x, ϕ_y, and ϕ are the components of rotation about coordinate lines and about the normal to the surface. (Fig 6)

The midsurface curvatures are:

$$K_x = \phi_{x,x} \tag{8}$$

$$K_y = \phi_{y,y} \tag{9}$$

$$2K_{xy} = 2K_{yx} = \phi_{y,x} + \phi_{x,y} + \phi/R \tag{10}$$

and in terms of displacements:

$$\phi_x = -W_{,x} \tag{11}$$

$$\phi_y = -W_{,y} + V/R \tag{12}$$

$$\phi = 1/2\ (U_{,y} - V_{,x}) \tag{13}$$

6

Through use of the Kirchoff-Love hypothesis and the orthoropic constitutive relations, the strain in any layer of the laminate can be expressed in terms of the previously derived midsurface strains and curvatures

$$
\begin{Bmatrix} \sigma_x \\ \sigma_y \\ \tau_{xy} \end{Bmatrix}_k = \begin{bmatrix} & Q & \end{bmatrix}_k \begin{Bmatrix} \varepsilon_x^{\,o} \\ \varepsilon_y^{\,o} \\ \gamma_{xy}^{\,o} \end{Bmatrix} + Z_k \begin{bmatrix} & Q & \end{bmatrix}_k \begin{Bmatrix} k_x \\ K_y \\ K_{xy} \end{Bmatrix} \qquad (14)
$$

where $[Q]_k$ is the transformed stiffness and is composed of:

$$
\begin{bmatrix} Q \end{bmatrix}_k = \begin{bmatrix} Q_{11} & Q_{12} & Q_{16} \\ & Q_{22} & Q_{26} \\ \text{sym} & & Q_{66} \end{bmatrix}_k \qquad (15)
$$

in which

$$
\overline{Q}_{11} = Q_{11}c^4 + 2(Q_{12} + 2Q_{66})s^2c^2 + Q_{22}s^4 \qquad (16)
$$

$$
\overline{Q}_{12} = (Q_{11} + Q_{22} - 4Q_{66})s^2c^2 + Q_{12}(s^4 + c^4) \qquad (17)
$$

$$
\overline{Q}_{22} = Q_{11}s^4 + 2(Q_{12} + 2Q_{66})s^2c^2 + Q_{22}c^4 \qquad (18)
$$

$$
\overline{Q}_{16} = (Q_{11} - Q_{12} - 2Q_{66})sc^3 + (Q_{12} - Q_{22} + 2Q_{66})s^3c \qquad (19)
$$

7

$$\bar{Q}_{26} = (Q_{11} - Q_{12} - 2Q_{66})s^3c^3 + (Q_{12} - Q_{22} + 2Q_{66})sc^3 \tag{20}$$

$$\bar{Q}_{66} = (Q_{11} + Q_{22} - 2Q_{12} - 2Q_{66})s^2c^2 + Q_{66}(s^4 + c^4) \tag{21}$$

where $s = \sin\theta$ and $c = \cos\theta$ (Fig 1). The angle θ being defined as the angle from the x axis of the body coordinate system to the 1 axis coincident with the fibers.

$$Q_{11} = E_1/(1-\nu_{21} \nu_{12}) \tag{22}$$

$$Q_{12} = \nu_{12}E_2/(1 - \nu_{12}\nu_{21}) = \nu_{21}E_1/(1 - \nu_{12}\nu_{21}) \tag{23}$$

$$Q_{22} = E_2/(1 - \nu_{12}\nu_{21}) \tag{24}$$

$$Q_{66} = G_{12} \tag{25}$$

By integrating through the thickness of the laminate and remembering midsurface strains and curvatures are not a function of z [3] the resultant forces and moments (per unit length) can be expressed as:
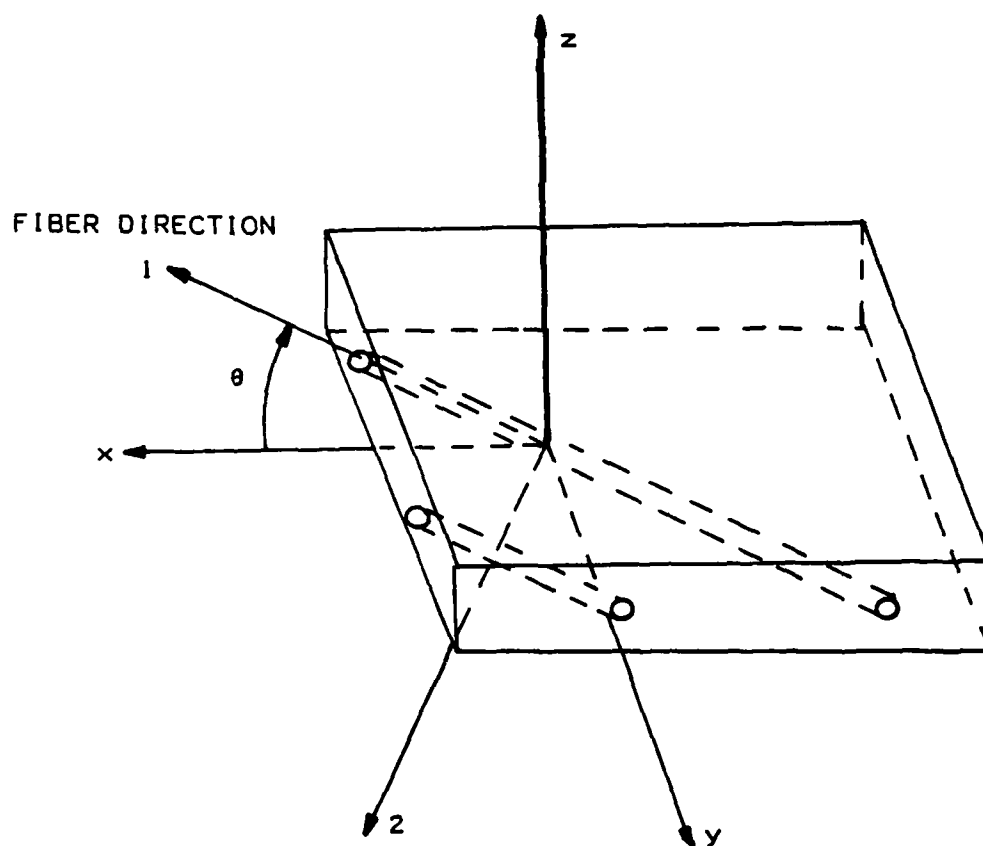
8

Fig 1: Rotation of Principal Axis

9

$$\left\{ \begin{array}{c} N_x \\ N_y \\ N_{xy} \end{array} \right\} = \begin{bmatrix} A_{11} & A_{12} & A_{16} \\ & A_{22} & A_{26} \\ sym & & A_{66} \end{bmatrix} \left\{ \begin{array}{c} \varepsilon_x^{\ o} \\ \varepsilon_y^{\ o} \\ \gamma_{xy}^{\ o} \end{array} \right\} + \begin{bmatrix} B_{11} & B_{12} & B_{16} \\ & B_{22} & B_{26} \\ sym & & B_{66} \end{bmatrix} \left\{ \begin{array}{c} K_x \\ K_y \\ K_{xy} \end{array} \right\} \quad (26)$$

$$\left\{ \begin{array}{c} M_x \\ M_y \\ M_{xy} \end{array} \right\} = \begin{bmatrix} B_{11} & B_{12} & B_{16} \\ & B_{22} & B_{26} \\ sym & & B_{66} \end{bmatrix} \left\{ \begin{array}{c} \varepsilon_x^{\ o} \\ \varepsilon_y^{\ o} \\ \gamma_{xy}^{\ o} \end{array} \right\} + \begin{bmatrix} D_{11} & D_{12} & D_{16} \\ & D_{22} & D_{26} \\ sym & & D_{66} \end{bmatrix} \left\{ \begin{array}{c} K_x \\ K_y \\ K_{xy} \end{array} \right\} \quad (27)$$

where $[A_{ij}]$ is the extensional stiffness matrix and is
defined as:

$$A_{ij} = \sum_{k=1}^{N} (\overline{Q}_{ij}) (Z_k - Z_{k-1}). \qquad (28)$$

$[B_{ij}]$ is the coupling stiffness matrix and is:

$$B_{ij} = 1/2 \sum_{k=1}^{N} (\overline{Q}_{ij})_k (Z^2_k - Z^2_{k-1}) \qquad (29)$$

and $[D_{ij}]$ is the bending stiffness matrix

$$D_{ij} = 1/3 \sum_{k=1}^{N} (\overline{Q}_{ij})_k (Z^3_k - Z^3_{k-1}). \qquad (30)$$

10

(See Figure 2 for sign notation for the forces and moments and Figure 3 for the geometry of the laminate.)

The strain energy of a panel can then be expressed in terms of moment and forces.

$$U = 1/2 \int_A \{\varepsilon\}^T \begin{bmatrix} N \\ M \end{bmatrix} dArea \qquad (31)$$

Or substituting equations 26-27:

$$U = 1/2 \int_A \begin{Bmatrix} \varepsilon_{xo}^{\,o} \\ \varepsilon_{y}^{\,o} \\ \gamma_{xy}^{\,o} \\ K_x \\ K_y \\ K_{xy} \end{Bmatrix} \begin{bmatrix} A_{ij} & B_{ij} \\ B_{ij} & D_{ij} \end{bmatrix} \begin{Bmatrix} \varepsilon_{xo}^{\,o} \\ \varepsilon_{y}^{\,o} \\ \gamma_{xy} \\ K_x \\ K_y \\ K_{xy} \end{Bmatrix} dArea \qquad (32)$$

The finite element is constructed from assumed displacements fields that serve as interpolation formulas. The exact and assumed displacement (interpolated curve) match at the nodes but may vary elsewhere. This however does not imply nodal values are exact [4]. The plate elements in STAGS C1 use an Hermitian interpolation in which the ordinates and slopes at the end po'nts of adjacent elements are forced to match. This operation results in an evaluation of the interpolation functions at the node ordinates. This results in the formulation of shape functions, H_i, which define displacements within an element when the ith element degree
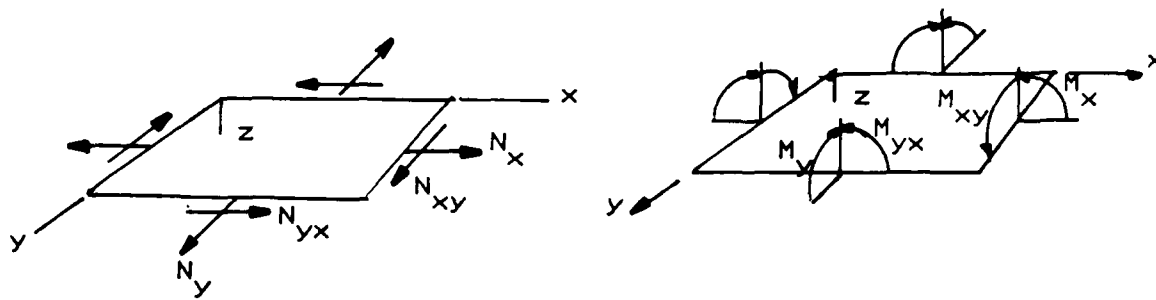
11

Figure 2:   Forces and Moments
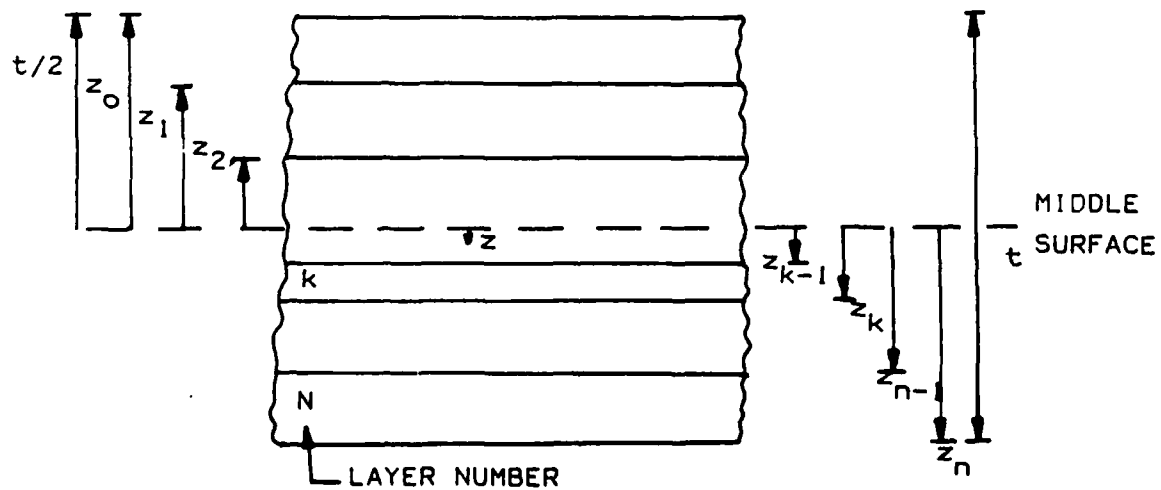
Figure 3:   Laminate Geometry

of freedom has unit value and all other degrees of freedom
are zero. The strains in equation (32) can be expressed in
terms of nodal displacements using the strain-displacement
matrix [G].

$$
\begin{Bmatrix} \epsilon \\ K \end{Bmatrix} = [G]\{d\} \tag{33}
$$

where [G] is a matrix populated with first order derivatives
for inplane strains and second order derivatives for bending
strains. Finally, substituting equation (33):

$$
\Pi = 1/2 \int_A \{d\}^T [G]^T \begin{bmatrix} A_{ij} & B_{ij} \\ B_{ij} & D_{ij} \end{bmatrix} [G]\{d\} \, dA \tag{34}
$$

The elemental stiffness matrix is then defined as:

$$
[k_{ij}] = \int_A [G]^T \begin{bmatrix} A_{ij} & B_{ij} \\ B_{ij} & D_{ij} \end{bmatrix} [G] \, dA \tag{35}
$$

and is superimposed with the other elemental stiffness
matrices to form the global stiffness matrix for the panel.

The mass matrix used in the STAGS C1 code is of a
lumped diagonal form [13]. Conceptually, lumping implies
that translational motion of a node is shared evenly by the
adjacent nodes. The mass can be thought of as equivalent
lumps at the nodes and the lumps have no rotary inertia.

13

The implication of zero rotary inertia is that zeros are located on the diagonal corresponding to rotational degrees of freedom. Lumped mass matrices are positive semi-definite if they have zeros in the diagonal. The implications being that convergence from above (computed natural frequencies greater than exact) cannot be assured. In fact, natural frequencies using lumped mass matrices usually yield natural frequencies lower than exact [4].

By defining the structural and mass properties in terms of displacements, the solution of equation (3) becomes that of an eigenvalue problem. For nontrivial solutions the determinant

$$[K_{ij}] - \lambda [M_{ij}] = 0 \tag{36}$$

where $\lambda = w^2$

The determinant results in the characteristic equations whose roots are known as eigenvalues (λ). Substitution of the eigenvalue into equation (36) results in a matrix of coefficients defining the eigenvector or natural mode. The eigenvector describes the relative displacements of the nodes in n-dimensional space. It is important to note that

14

the eigenvector only defines relative displacements. Hence,
the shape of the natural modes is unique, but not the
amplitude [7].

Holographic Interferomety

A hologram is formed when two sets of spatially
coherent light waves are made to interfere on a photographic
medium. The light wave originating at a single light source
is split between two paths; one illuminating the object
being recorded, the other serving as a reference to the
original coherent wavefront. The wave front reflected from
the recorded object is irregular and very complicated. On
the reference path the spatial coherence is retained. The
two paths intersect again at the photographic plate (Fig 4)
creating a complex interference pattern. The interference
is of two types, constructive and destructive. When the two
wavefronts meet at a point in phase, the total amplitude
increases constructively as the sum of the individual
amplitudes. Similiarly, when the two wavefronts are not in
phase a destructive or diminishing effect occurs in the
amplitude. This interference pattern, known as a field, is
recorded on the photographic plate during the exposure. The
points where constructive interference occurs form parallel

15

dark fringes on the order of 5×10^{-4}mm [5] and are not

visible to the eye. After the plate is developed and fixed

these fringes become the hologram and act much like a wave

grating [16]. When this hologram is illuminated by a

coherent light source identical to the reference beam, the

fringes diffract the light into wavefronts essentially

indistinguishable from the waves which were reflected from

the object. (Fig. 5) The diffracted waves produce all the

optical characteristics of phase and amplitude of the

original waves [5]. This image differs dramatically from a

normal photograph which is essentially a spatial recording

of light intensity on the film.

Conducting vibration analysis with holography requires

a time averaging technique. The panel is excited (in this

case acoustically) at a natural frequency and the object

assumes a modal vibration pattern. The photographic plate

records all fields that existed during the exposure time in

proportion to the fraction of time during which the

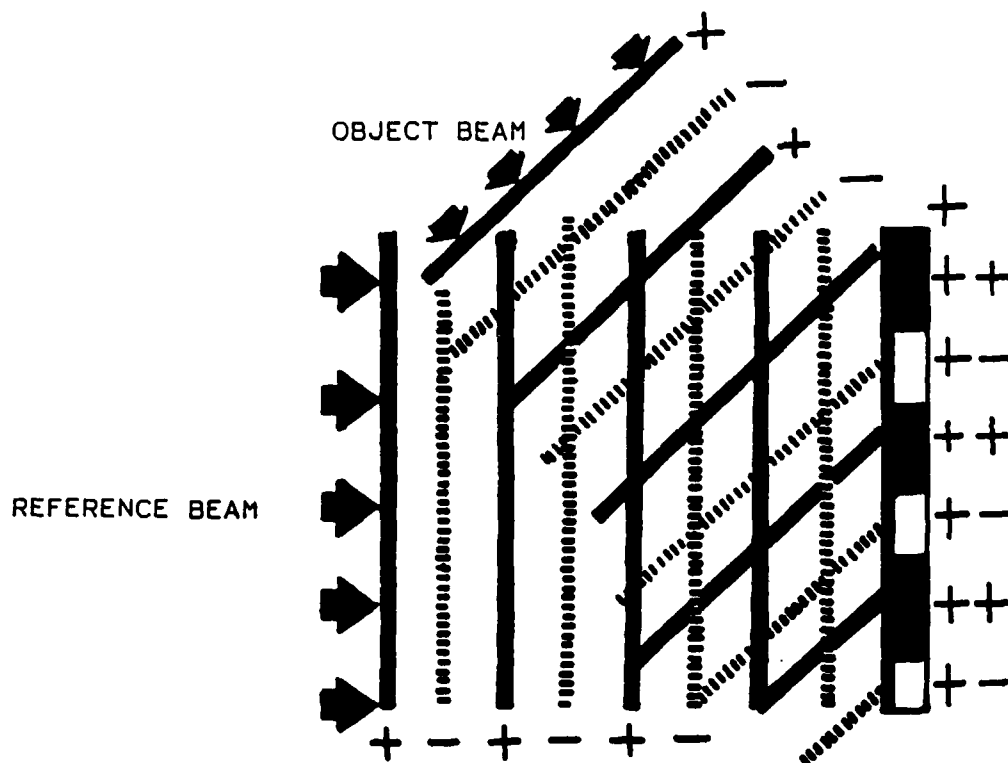wavefront existed. Even though the fields are reconstructed

16

OBJECT BEAM

REFERENCE BEAM

Figure 4: Fringe Formation

UNDEVIATED WAVES

REFERENCE BEAM

RECONSTRUCTED WAVEFRONT
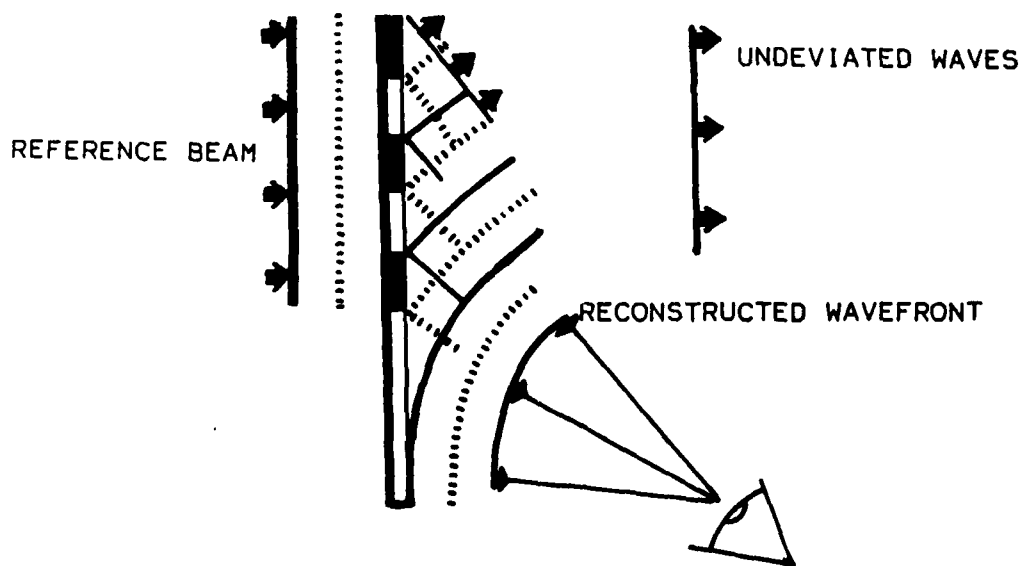
Figure 5: Hologram Reconstruction

17

simultaneously by the reference beam [5]. Thus, when viewed
by an observer, a pattern of broad fringes, much greater in
size and clearly visible to the eye, appear on the object
image. Due to the interference between the fields, these
broad fringe lines connected points of constant deflection.
It should be noted at this point that only the out of plane
displacements are recorded in this manner and care must be
taken to avoid interpreting similiar deflection patterns on
a single body as necessarily indicating the same mode.   Two
modes may have similiar out-of-plane displacements yet have
in-plane displacements which are dramatically different
[14].

III. MODELLING

Panel Properties.

The graphite/epoxy shell study in this thesis was cylindrical in shape with a height of 16 inches, a chord length of 16 inches, and a radius of curvature of 12 inches. The shell dimensions and sign convention used in the STAGS program are shown in (Fig 6). The panels were eight quasi-isotropic layups. [0, -45, +45, 90]s, of Hercules 3501/AS graphite epoxy. Each ply is approximately .005 inches thick for a total laminate thickness of .04 inches. The cure cycle can be found in Appendix B. The fabrication was conducted by personnel at the Air force Flight Dynamics Laboratory as were the material property tests. These tests determined the material properties of the material as:

$$E_1 = 18.84 \times 10^6 \text{ PSI}$$
$$E_2 = 14.68 \times 10^5 \text{ PSI}$$
$$G_{12} = 9.099 \times 10^5 \text{ PSI}$$
$$\nu_{21} = 2.1813 \times 10^{-2} \qquad \nu_{12} = .2799$$
$$\rho = .055 \text{ lb/in}^3$$

These parameters were an input to the STAGS-C1 code. It should be noted that the User's Manual for STAGS calls for

19
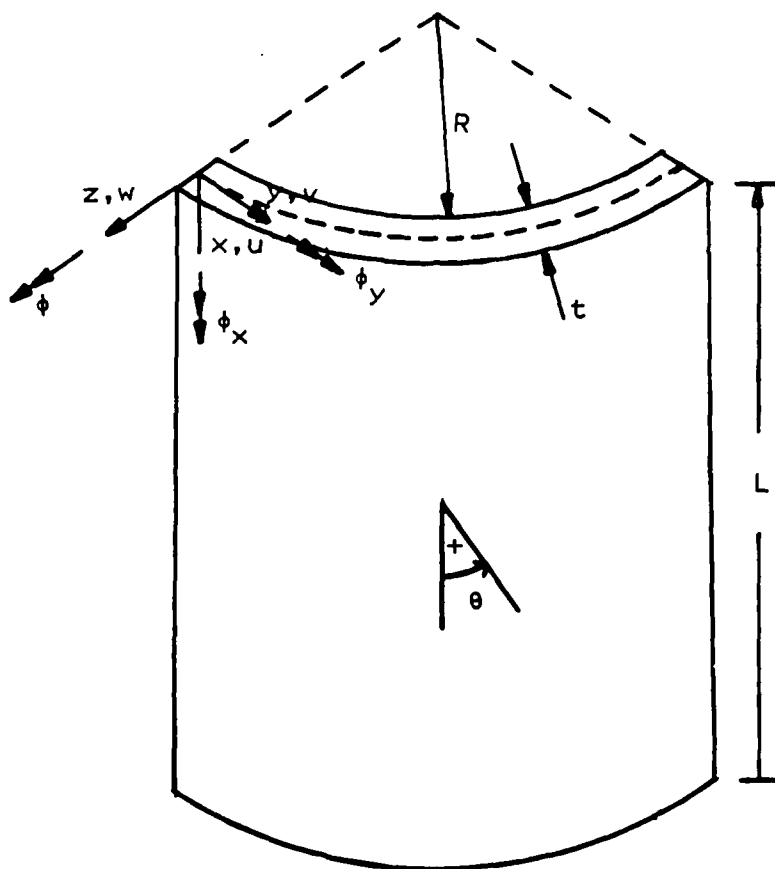
t = thickness = 8 plies @ 0.005" = 0.04"

R = radius = 12"

C = width = chord length = 16"

L = length = 16"

x,y,z = structural coordinate directions

θ = ply orientation

u,v,w = displacements

ϕ_x, ϕ_y, ϕ = rotations

Figure 6: Panel Notation

20

ν_{12}, but this notation is contrary to that found in most references for composite materials. The property expected by STAGS is ν_{21} in conventional notation

$$\nu_{21} = -\varepsilon_2/\varepsilon_1 \qquad (37)$$

Where ε_2 is defined as the strain normal to the fiber direction and ε_1 is defined as strain in the fiber direction.

Element Selection

Curved shell elements require large amounts of computer time for formulation of the stiffness matrix. Also the use of a curved element can induce strain under rigid body motion [8]. Thus, the approach used by the STAGS code is to use flat plate elements. These QUAF elements incorporate both in-plane and bending degrees of freedom. Modelling a shell with flat plate elements can result in element nonconformity between adjacent elements. The flat elements meet at angle and a normal rotation degree of freedom is added at the corner nodes to enforce rotational compatibility of element boundaries [Fig. 7].

21

This implies:

$$(\beta_{y1} - \beta_{y2})\cos(\alpha/2) - (\beta_{z1} + \beta_{z2})\sin(\alpha/2) = 0$$

$$(\beta_{z1} - \beta_{z2})\cos(\alpha/2) - (\beta_{y1} + \beta_{y2})\sin(\alpha/2) = 0 \tag{38}$$

where:

β_y = rotation about y coordinate line

β_z = rotation about z coordinate line

α = angle between elements

The STAG-C1 code defines a small limit α_0 and if $\alpha < \alpha_0$, the rotation β_z is ignored and as an approximation the conformity constraint becomes $\beta_{y1} = \beta_{y2}$ [8].

A more serious problem is caused by interelement displacement compatibility. The assumed displacement fields for the in-plane displacements, u and v, contain first order derivatives while the transverse displacement field for w contains second order derivatives. Therefore, w is usually represented by higher order ploynomials than u and v. Because the elements meet at an angle, compatibility between the boundaries of adjacent elements require that:

$$(v_1 - v_2)\cos(\alpha/2) - (w_1 + w_2)\sin(\alpha/2) = 0$$

$$(w_1 - w_2)\cos(\alpha/2) + (v_1 + v_2)\sin(\alpha/2) = 0 \tag{39}$$

This condition cannot be met unless the displacement
polynomials are of the same order. The STAGS-C1 QUAF
elements alleviate this problem by including normal rotation
components $u,_y$ and $-v,_x$ at the corner nodes. The inclusion
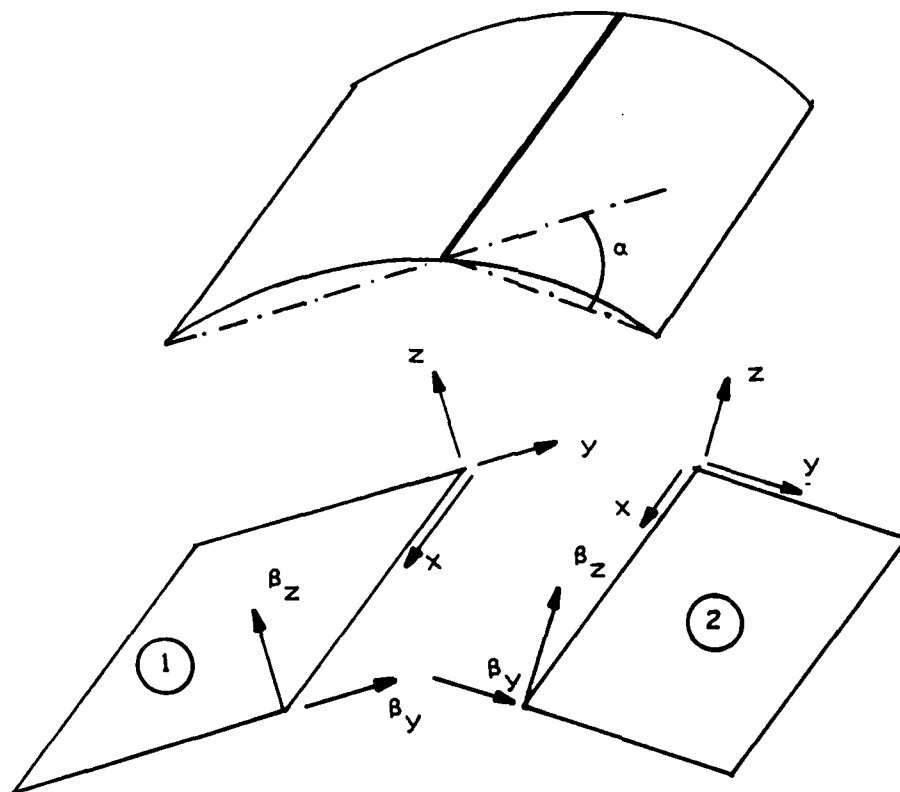

Figure 7: Rotational Compatibility

23

of these displacement derivatives as degrees of freedom result in an in-plane displacement field that is cubic for displacements normal to element boundaries. The displacements tangential to the element boundaries are made quadratic by raising the order of u in the x direction and v in the y direction through the addition of tangential degrees of freedom at midside nodes. The midside nodes allow linear strain tangential to the boundaries and alleviate the slow convergence found with constant strain elements [8]. The complete set of shape functions in isoparametric form can be found in [8]. The STAGS-C1 QUAF 411 incorporates these 7 degrees of freedom at the corner nodes and 1 degree of freedom at each of the midside nodes for a total of 32. (Fig 8) A simpler QUAF 410 element (Fig 9) is available that eliminates the side nodes and uses only an average normal rotation at corner nodes. This reduces the element to constant strain capability tangential to the boundaries and suppresses shear strain at the corner nodes. Consequently one would expect faster convergence with fewer elements when modelling curved surfaces with the QUAF 411 element.
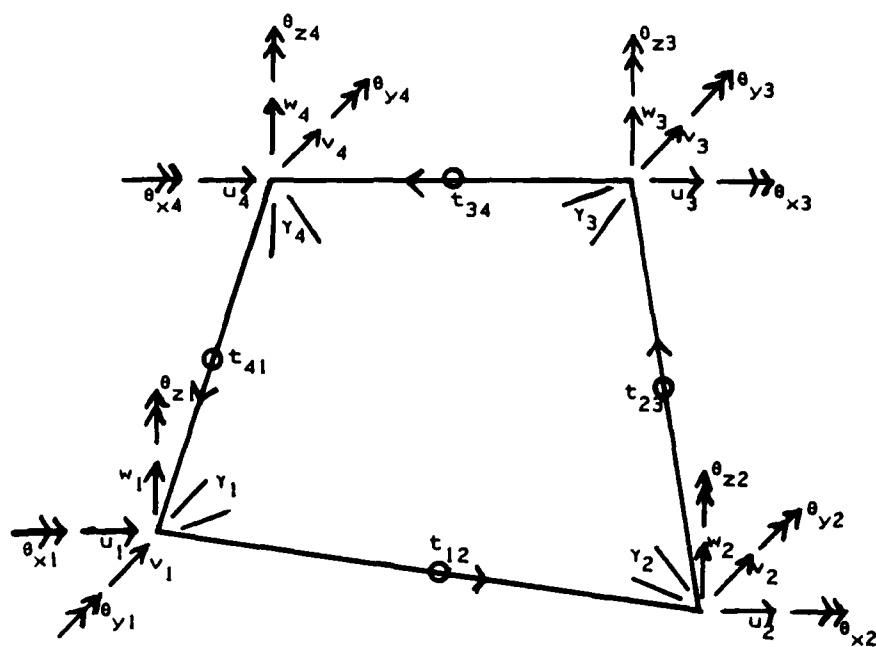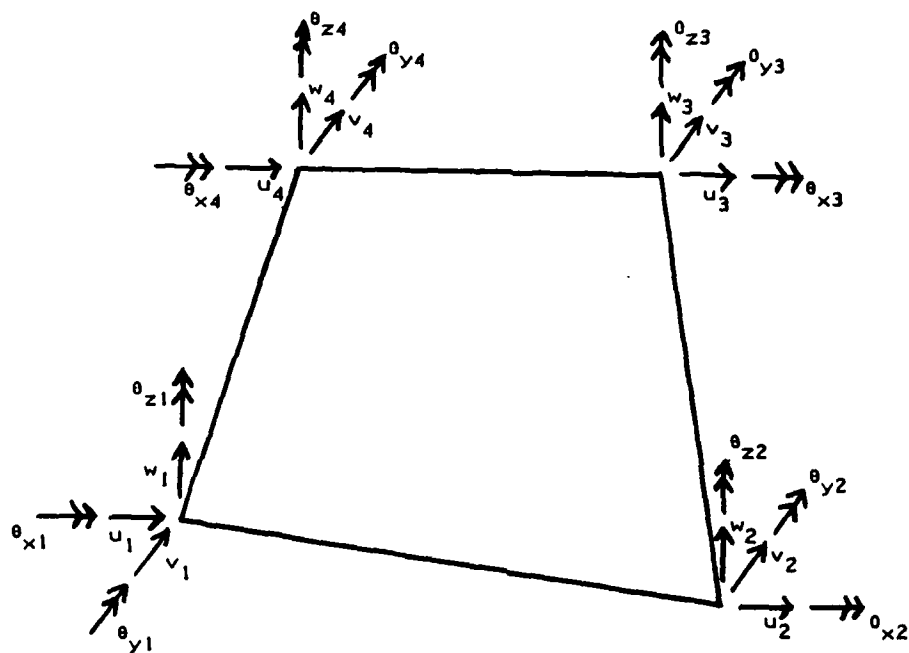
24

Figure 8:   QUAF 411

25

Figure 9:   QUAF 410

IV. FINITE ELEMENT ANALYSIS

Defining the Element Grid

At the beginning of this effort, it was felt that the QUAF 411 plate element would be required to model the curved surface of the panels. This decision was based on the normal degrees of freedom added to this element to insure compatibility between element boundaries subject to shear. The interelement compatibility requirement and higher order normal strain (linear vs constant) function were predicted to provide faster convergence with fewer elements. A potential liability of this choice was that the 32 degrees of freedom and nine point numerical integration utilized by the 411 element versus the 24 degrees of freedom and 5 point integration of the 410 [8] element would require greater computer resources for the same grid size. This was of particular concern due to the desire to utilize a digital VAX 11/780 computer operating under the VMS operating system for analysis.

A convergence study was conducted using a 32 x 13, 19 x 19, and 25 x 25 square element grid for the solid shell. This results in a constant 1.0, 0.75, and 0.5, inch grid line spacing respectively. The results are tabulated below for the fundamental frequency.

27

GRID	411 Computation Time		410 Computation Time	
	FREQ	CPU sec	FREQ	CPU sec
13 x 13	364 Hz	698	365 Hz	439
19 x 19	460 Hz	2355	461 Hz	1413
25 x 25	504 Hz	5844	506 Hz	3019

Element Comparison

Table 1

It is apparent that the anticipated benefits of the 411
element did not materialize. The computed fundamental
frequencies varied by less than 0.5 percent. The other
result of interest lies in the difference in computation
time. The computation time for the 411 element is 37
percent greater for the 13 x 13 grid and 48 percent greater
for the 25 x 25 grid. The 410 element appears to provide
virtually identical results with a substantial cost savings.
The failure of the 411 element to exhibit faster convergence
suggests that for the clamped-clamped boundary conditions
the higher order displacement fields are ineffective. This
can be explained by reviewing the displacement fields of the
additional degrees of freedom found in the 411 element. The
corner node rotation is added to the element as derivatives
of inplane displacements with respect to the normal ordinate

28

i.e., $U,_y$ and $V,_x$. The midside nodes also add only to the order of the inplane displacement fields. Considering the boundary conditions, the small vibration problem is primarily one of out-of-plane displacements. Thus, the additions to the order of the inplane displacements add little to the solution of this particular problem. The QUAF 410 element was judged best for this problem.

To insure the grid size had been reduced to a point where the tradeoff between accuracy and computation time had reached an acceptable level, a computer run utilizing a 31 × 31 square grid was submitted. This run failed to converge to acceptable error limits for the fifth eigenvalue before the alloted disk space on the VAX 11/780 was exceeded. However, the fundamental eigenvalue had converged and was determined to be 529 Hz. This is a change of approximately 5 percent, and the 25 × 25 grid was established as the best balance between accuracy and computer resources.

As indicated in the previous discussion, a decreasing grid mesh results in greater computed natural frequencies. Since the finite element model is an approximation utilizing a finite number of degrees of freedom to model an essentially infinite number found in the actual structure, the model should always be expected to possess greater

29

stiffness. Given the same mass, the model would then be expected to yield higher natural frequencies with increasing grid spacing (fewer degrees of freedom). Conversely, as the spacing is refined the computed frequencies should decrease or converge from above to the exact value. The behavior indicated in this analysis would then imply some error in the model. As mentioned in the theory discussion, the lumped mass matrix frequently causes the results to converge from the bottom. This behavior was also observed in an evaluation of the STAGS C1 code by the Office of Naval Research [15]. This study noted that while the convergence problem indicated a failure to satisfy some equations of mechanics, the results were not adversely affected.

Panel Analysis

Having determined the grid size to be used for each panel, an input file for each of the panels was constructed. The cutouts were entered using the IRREG parameter on the N-1 input card. Then the N-8 input card allows the user to define rectangular cutouts in terms of grid coordinates [6]. The 2 x 2 inch square being defined row 11-15, column 11-15; the 2 x 4 cutout row 11-15, column 9-17; the 4 x 4 cutout row 9-17, column 9-17. To facilitate the plotting of the

30

eigenvectors, the z axis of the global reference system was
chosen to intercept the midpoint of the chord of the panel.
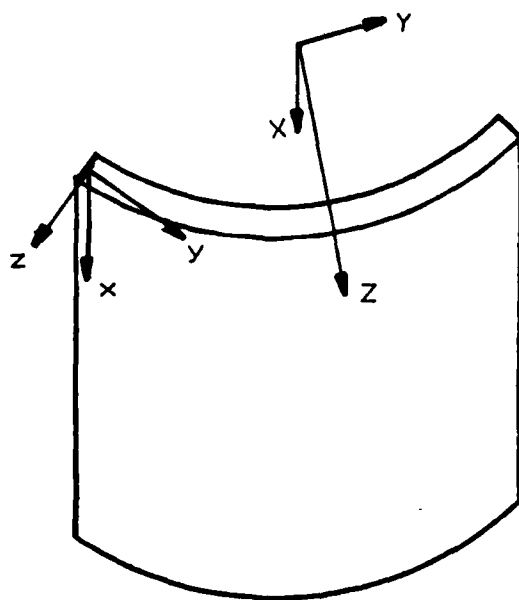(Fig 10).

Figure 10:   Global Coordinate System

This placement allowed the displacements expressed in terms
of the local curvilinear system to be easily rewritten based
on the global system. This conversion was conducted using
the expression

$$w \cos(y) + v \sin(y) = W \qquad (40)$$

Where y = local coordinate (degrees)

w = local normal displacement

v = local transverse displacement

W = global displacement

The transformed displacements could then be plotted using a
contour plot algorithm and provide the same perspective of
mode shape found in the holograms. The global system was
fixed by inputing the appropriate global value for the
extreme corner points as required by STAGS. Remembering the
Y coordinate line is expressed in terms of degrees the
following comparison is included.

32

Corner Points		Local System		Global System		
Row	Col	x	y	X	Y	Z
1	1	0.0	-28.65	0.0	-5.75	10.53
1	25	0.0	28.65	0.0	5.75	10.53
25	1	12.0	-28.65	12.0	-5.75	10.53
25	25	12.0	28.65	12.0	5.75	10.53

Global System Definition

Table 2

A sample input file for a panel with and without a cutout is
included in Appendix A.

Numerical Solution

The STAGS-C1 code utilizes an inverse power method to
evaluate the roots of equation (36). This method [4]
rewrites equation (36) as:

$$[K] - \lambda_0[M] \{D\}_p = [M] \{D'\}_{p-1} \tag{41}$$

$$\{D'\}_p = D_p/C_p \tag{42}$$

where

λ_0 = shift point

C_p = largest magnitude of vector $\{D\}_p$.

33

The algorithm assumes a vector solution $\{D'\}_0$ (p=1) to solve equation (41) for $\{D\}_1$. $\{D\}_1$ is then scaled using equation (42) to get $\{D'\}_1$ which in turn is reiterated in equation (41). This iterative method converges to the eigenvalue closest to the shift point λ_0. Since in this analysis the lowest five eigenvalues were desired, the shift point (SHIFT on input card D-3) was chosen as zero. The iteration values can be included as part of the program output (IPRINT on D-2 card). The eigenvalues are then used to evaluate equation (36) to determine the eigenvectors. The program lists the displacements in tabular form at each grid point. These displacements were edited in a short Fortran routine using equation (42) and the displacement values rewritten in the data field format required by the contour plot routine. The plot routine was then exercised to provide a visual outline of the mode shape at each natural frequency.

V. HOLOGRAPHIC ANALYSIS

The Test Fixture

In order to conduct the holographic analysis, a test
fixture capable of supplying clamped boundary conditions on
both the flat and curved edges of the cylindrical shell was
needed. In addition, the test fixture had to remain stable
over the frequency range of interest and under temperature
changes that might occur during testing. The extreme
sensitivety of the holographic method is quite capable of
recording rigid body motion of the test fixture due to
thermal effects or vibration. This rigid body motion would
be superimposed on the panel motion and would be impossible
to distinguish. Steel was chosen over aluminum due to its
lower coefficient of thermal expansion. greater stiffness,
and mass. The fixture was designed and constructed to
provide a two inch clamping surface on eac. jge. The
vertical clamps were constructed (Fig 11) f a 12 inch
sections of 4 x 4 inch bar stock. A 2 1/8 x 1 1/2 path was
milled from one face of each bar to form a U shaped
structure. Two rows of quarter inch holes were drilled and
tapped along each side for clamping bolts. These bolts
tightened against 1/2 x 2 x 12 inch flats placed on each
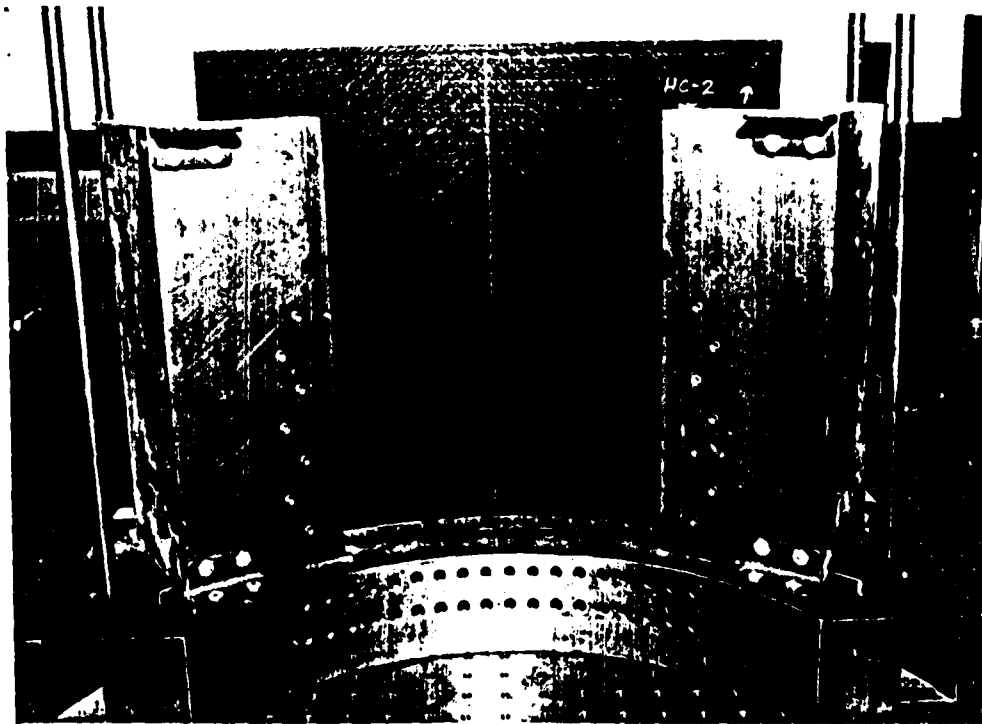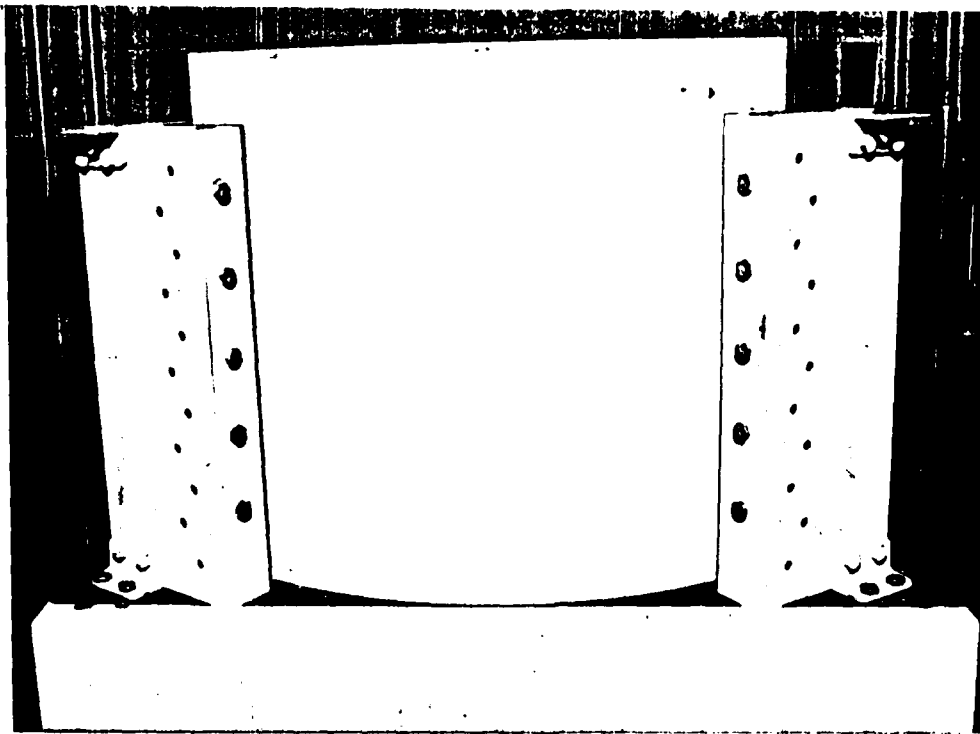side of the graphite/epoxy panel. When the bolts on each

35

Figure 11A: Test Fixture
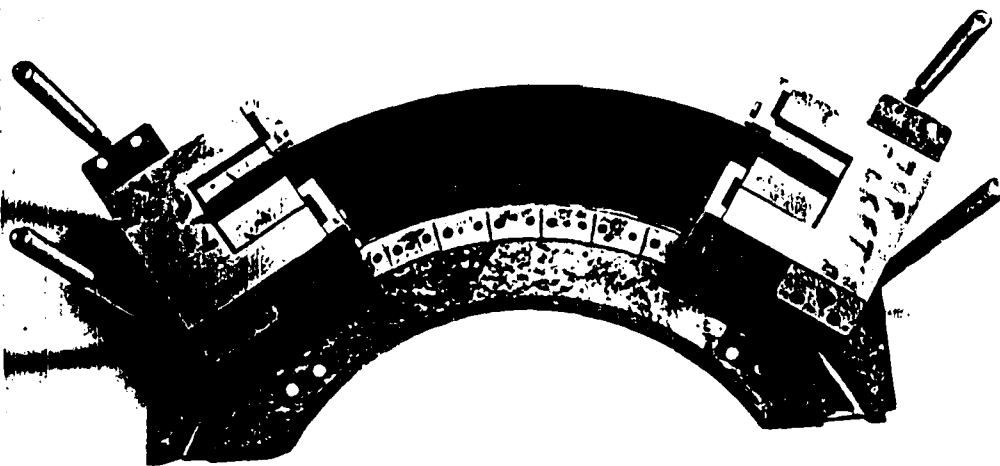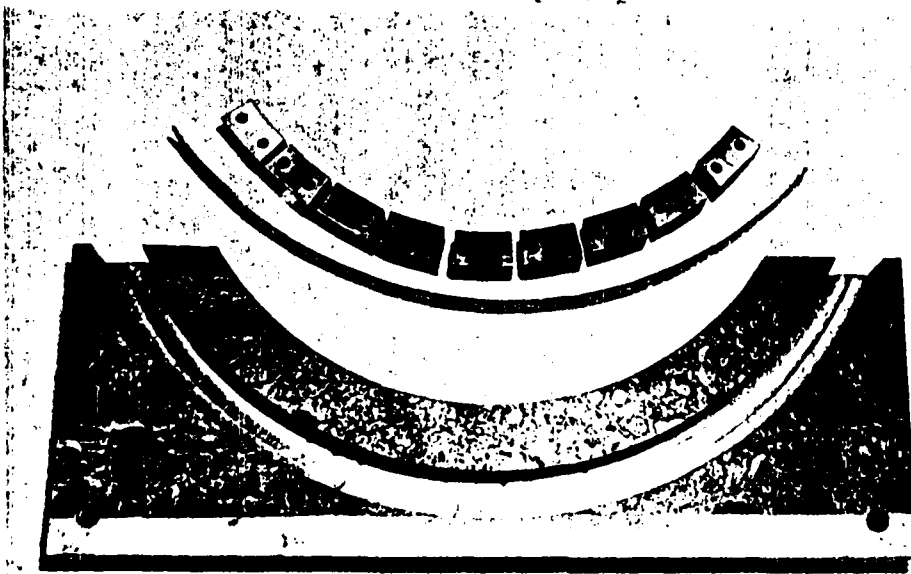
36

Figure 11A: Test Fixture

36

Figure 11B: Test Fixture

37

side of the clamp were tightened the panel was securely
clamped between the flats. To prevent lateral motion
smaller U shaped clamps were installed on the open face of
the vertical clamps. A curved 1 1/4 inch wide by 2 1/8 deep
path with an outer radius of twelve inches was milled from a
22 inch wide by 10 inch deep by 3 inch thick steel stack.
The twelve inch outer radius matched that of the panels. A
set of 9 curved blocks, 1 inch thick, 2 inches in height,
and 1 3/4 inches in chord were milled to match the inner
radius of the panels. Great difficulty in accurately
machining these blocks lead to a decision to add a thin
(40 mils) ductile aluminum bushing between the outer radius
of the block sets and the panel. It was felt that this
bushing would evenly distribute clamping forces between
clamping blocks. Transverse motion here was prevented by
milling two lateral grooves to match the contact points of
the clamping bolts. The paths for these bolts were drilled
and tapped radially on the inner radius of the horizontal
flats. Four 1/2 inch rods were added to provide structural
rigidity and act as assembly aids when changing panels.
When assembling the fixture, the two vertical clamps and
bottom section were joined and the panel inserted between
clamping surfaces. The top flat was then installed and the
radial clamping blocks were inserted from the concave side.

38

Each clamping bolt was tightened to 6 ft-lbs. This fixture
appeared to provide a very good approximation of the clamped
boundary conditions that were desired. In none of the
holography experiments were fringe lines ever observed to
extend into clamp. Such a fringe line would have indicated
a line of displacement extending into the clamp and thus
poor clamping.

Experimental Procedure

The equipment used in the experiment is listed below:

Function Generator:	H P Model 3310B
Frequency Counter:	H P Model 5316A
Audio Amplifier:	Bogen Model HTA125
Fotonic Displacement Meter:	Mechanical
	Technology KD 320
Oscilloscope:	Tektronix 7603
50mV Helium/Neon Laser:	Spectre Physics
	(Model 125)
Acoustic Drivers:	Atlas Sound 60 Watt

A block diagram of the equipment configuration is shown in
Fig (12). The optical set up is shown in Fig (13). In order
illuminate the entire area of the panel and photographic

39

plate, 20X microscope objectives were employed to expand the beam. Pinhole spatial filters are used in series with the objectives to eliminate refractive fringes due to dust particles on the mirrors.

Real time holographic interferometry was used to determine the natural frequencies and mode shapes of the four panels. The procedure involves making a hologram of the stationary panel. The hologram is then placed in the plate holder in the position in which it was formed. When this hologram and the object are illuminated, their images are coincident. When the panel is excited at resonant frequency by the acoustic drivers, it assumes a corresponding mode shape. The two images are no longer coincident. Thus, broad fringe bands are formed on the image into a pattern which resembles that of the associated mode shape. The procedure then becomes one of sweeping through the frequency range until a pattern appears on the image. To preclude the possibility that the pattern induced by the input signal of the acoustic drivers is not actually a response to a multiple (harmonic) of that frequency, an optical displacement meter was employed to determine panel response. By comparing the output signal of the optical displacement sensor to that of the acoustic signal, the Lissajous pattern that results on the oscilloscope was used

40

to confirm that the panel was actually vibrating at the acoustic frequency. For example, a harmonic response to a 60 Hz input signal may actually be occurring at 480 Hz. To the viewer of the hologram, the displacement patterns are identical but the Lissajous pattern would actually display 8 lobes. The displacement sensor had two advantages over an accelerometer often employed in this instance. The optical probe was easily moved about the face of the panel without having to break any bonding glue. The second advantage, particularly for vibration analaysis, is that the optical technique does not add mass to the structure. The added mass associated with accelerometers actually charges the response of the structure during the analysis.

In this experiment, two identical acoustic drivers with exponentially convergent cones were used to excite the panels. Two horns, driven 180 degrees out of phase, were required to excite mode shapes that were antisymmetric about the vertical line of symmetry of the curved panel. This push-pull excitation was particularly necessary when a symmetric and antisymmetric mode shapes occurred at relatively close frequencies. It should be noted that the horns used in the experiment were approximately 6 inches in diameter and thus, could not be placed on the same horizontal plane and still excite the concave surface of the

41

panels.   The horns had to be placed at opposing corners and
thus were not capable of a true antisymmetric excitation.
This proved to be of minor consequence as discussed in the
next section.

After using the real time technique and optical
displacement sensor to determine natural frequencies, a time
average hologram was constructed to permanently record each
mode shape.   The mode shapes and frequencies were then
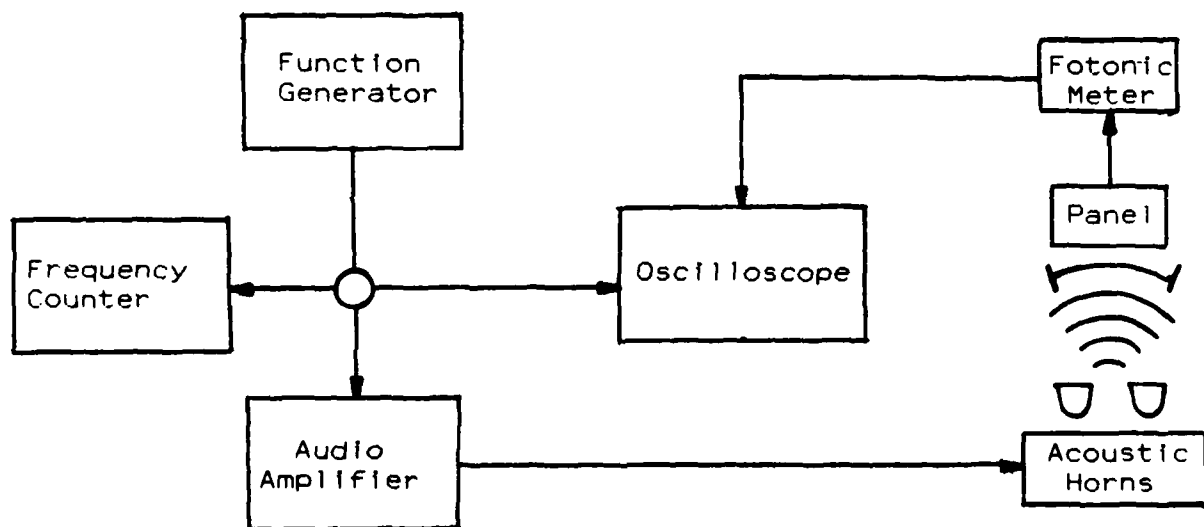compared with numerical results.

42

EQUIPMENT SETUP
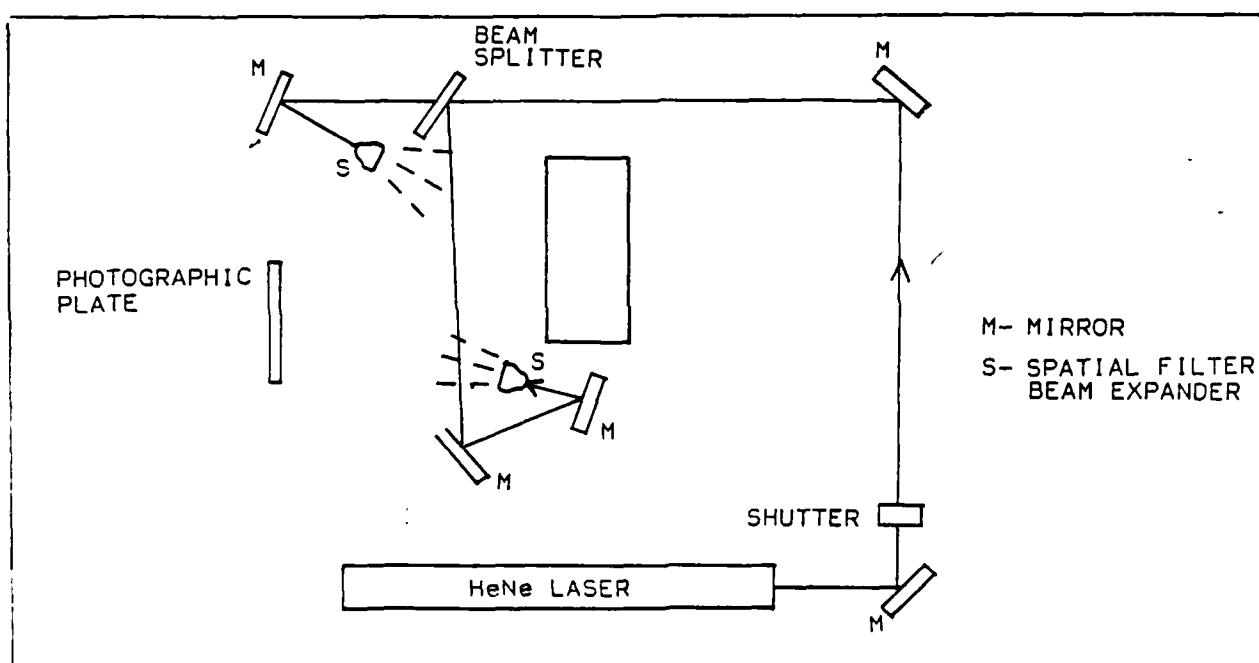

Figure 12: Equipment Configuration

43

BEAM
SPLITTER

M

M

S

PHOTOGRAPHIC
PLATE

M— MIRROR

S— SPATIAL FILTER
BEAM EXPANDER

S

M

M

SHUTTER

HeNe LASER

M

Figure 13:   Optical Configuration

44

VI. DISCUSSION AND RESULTS

This chapter is divided into four sections. It is
important to note that the comparrison offered here is
between experiment and numerical approximation. Therefore,
errors both positive and negative can be expected. Had the
comparison been a closed form or exact solution, the grid
spacing would be expected to predict values less than exact
under all conditions. The experimental test fixture can
only approximate clamped conditions that are modelled
exactly in the finite element solution. Thus, both
solutions studied here are approximations of the exact
solution and no trend in error should be expected. The
results for each of the four panels are discussed in order
of increasing cutout size.

The Solid Panel

The solid panel, its shape being the simplest, was
chosen first for both the numerical and experimental
analysis. Since the lowest five natural frequencies were
sought, the frequency range of investigation started at zero
and progressed upward until all five frequencies were found.
Excitation was provided by a single horn aimed at the center

of the panel. The solid panel was particularly susceptible to displaying harmonics. Using the real time holographic technique, an identical modal displacement pattern was seen to repeat itself between 0 and 534 Hz. Through use of the optical displacement meter, it was determined that each of the identical displacement patterns below 534 Hz were harmonic responses. This technique established that the true natural frequency was indeed 534 Hz. It was possible to visibly observe this process by scanning the frequency range at reduced sound levels from the acoustic horn. The harmonic responses would not appear at sound levels that would easily excite the true mode. The existence of harmonics is the result of exciting the panel with point sources such as the acoustic horns equipped with the exponential horns.

Scanning the frequency upward, it became evident that only those natural frequencies with mode shapes symmetric about the vertical midplane were being excited. A second horn, with input leads switched to produce a response 180 degrees from the other, was added to produce an antisymmetric excitation. Scanning again from zero, a modal response antisymmetric about the vertical midplane was found at 525 Hz. It was also found that the symmetric mode at 534 Hz could also be excited with the dual horn arrangement.

The small difference in these two natural frequencies, 1.7

percent, resulted in smearing of mode shapes in the hologram

as the frequency gap was traversed. This can easily be

explained due to the fact that, while the natural

frequencies are discrete values mathematically, the panel

would respond similiarly to a small range of frequencies

about that point. For these two frequencies, the ranges

were observed to overlap. The frequency scanning was

continued in this manner until the first five modes were

found. A general observation can be made at this point that

those mode shapes exhibiting symmetry about the vertical

midplane were always easier to excite.

SOLID PANEL

Mode	Frequency (Hz)		Percent
Number	STAGS	Experiment	Error
1	506	525	-3.6
2	524	534	-1.9
3	693	724	-4.3
4	703	736	-4.5
5	769	862	-10.8

Table 3

47

The mode shapes determined by the finite element method and holographic interferometry are presented in Figures 14-18. The fringes represent lines of constant displacement and can be interpreted much like a topographical map. The white areas which represent nodal lines or zones of zero displacement can be deduced from the fact that displacement is zero at the edges.

As a comparison of the photographs and contour plots shows, the mode shape predictions for the solid panel by the STAGS-C1 program are quite accurate. The slight tilting of the lines of constant displacement toward the upper left is visible in both the holograms and contour plots. This effect appears to be a bias toward the +45 degree direction which, in this laminate, corresponds to the fiber layers closest to the midsurface 90 degree lamina. While no explanation for this behavior is evident, its occurrance in both cases indicates it is real and not an effect of boundary conditions of test fixture. Similiarly, the error in predicting the natural frequency is quite low.

The 2 x 2 Inch Cutout

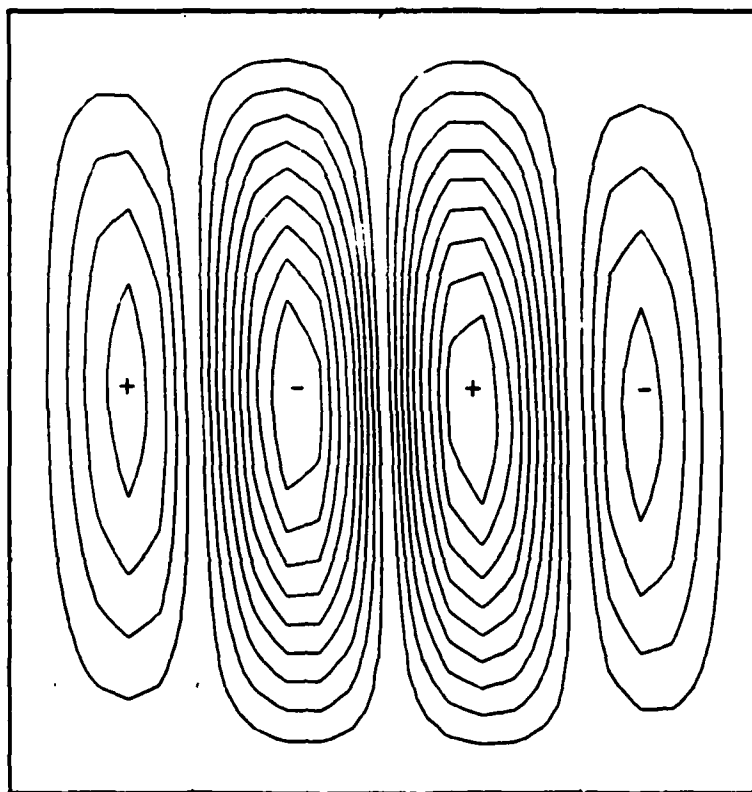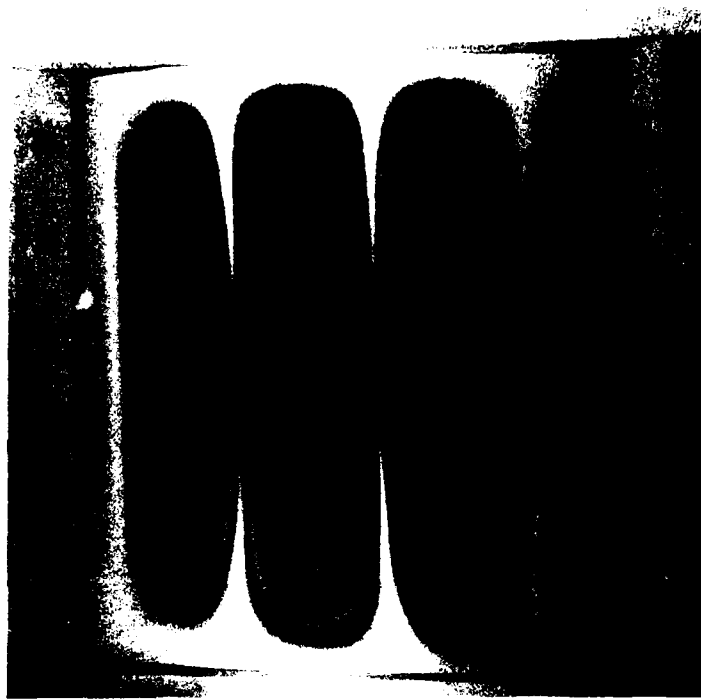As with all the panels, the procedure employed to find natural frequencies was identical to that used for the solid
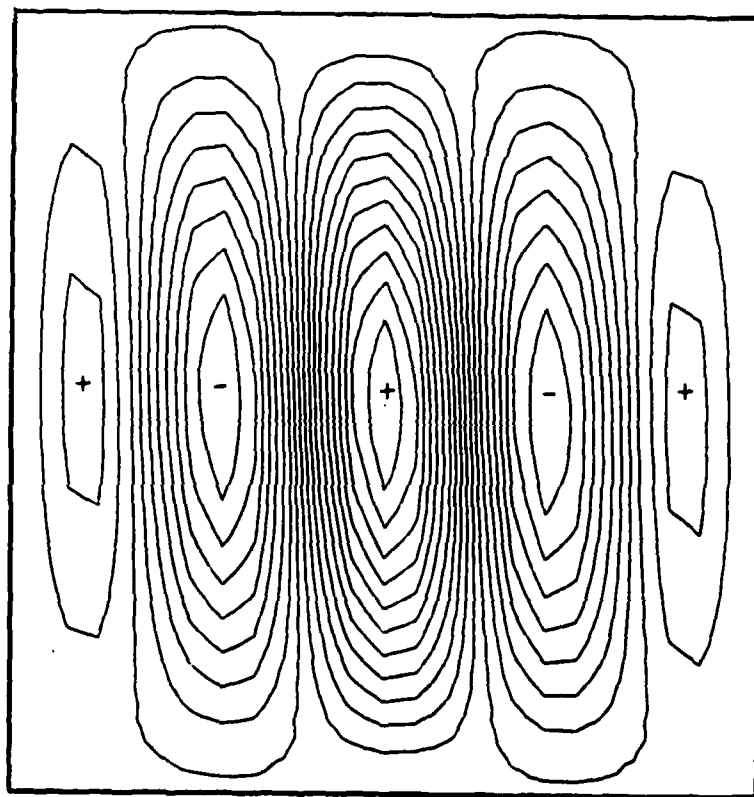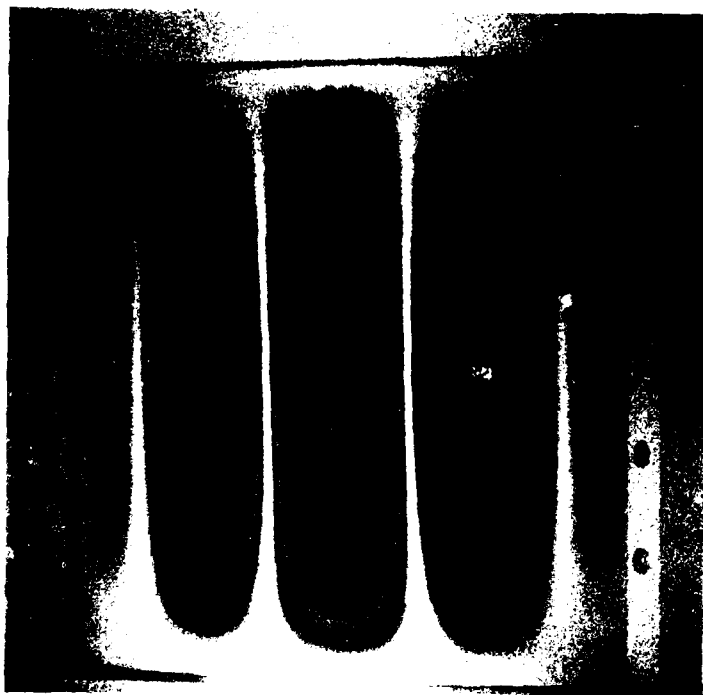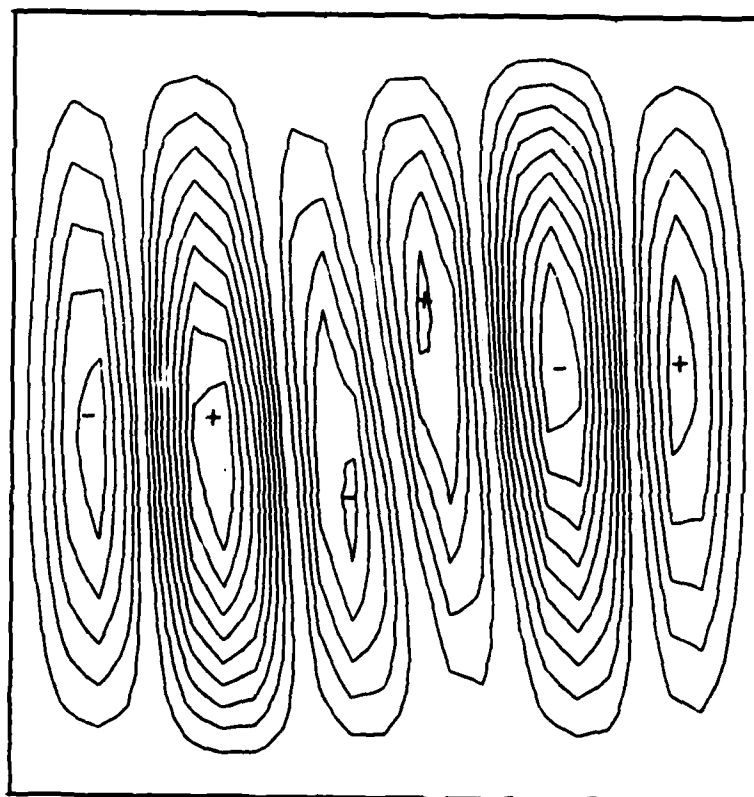
Figure 14:   Solid Panel Mode 1
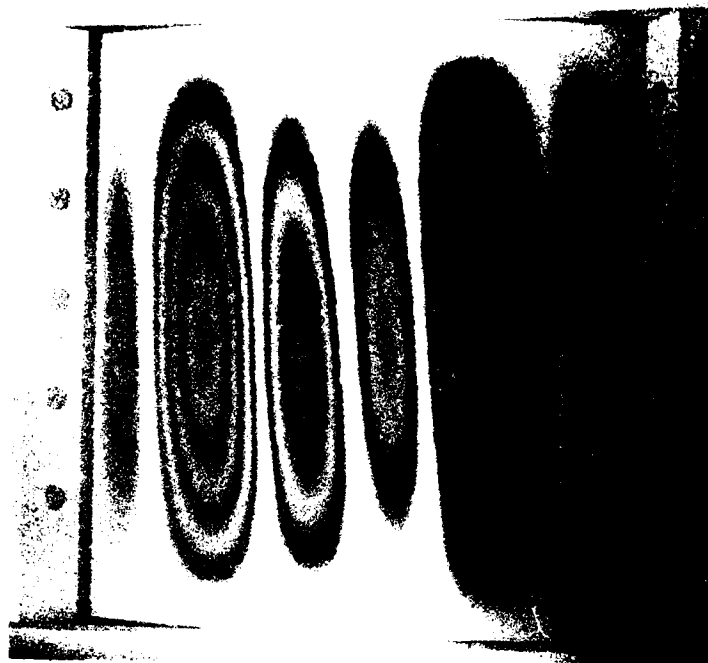
Figure 15:   Solid Panel Mode 2

50

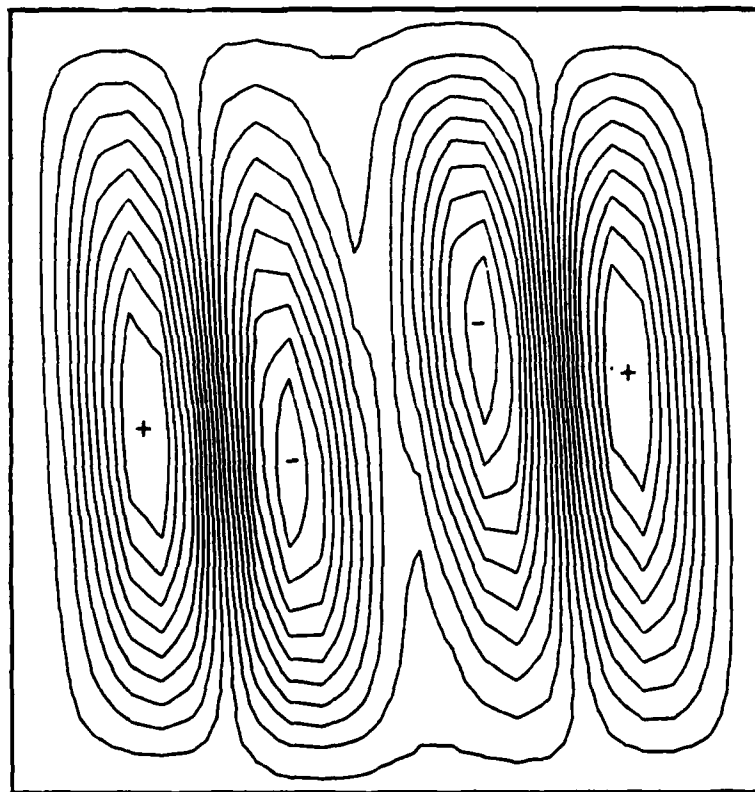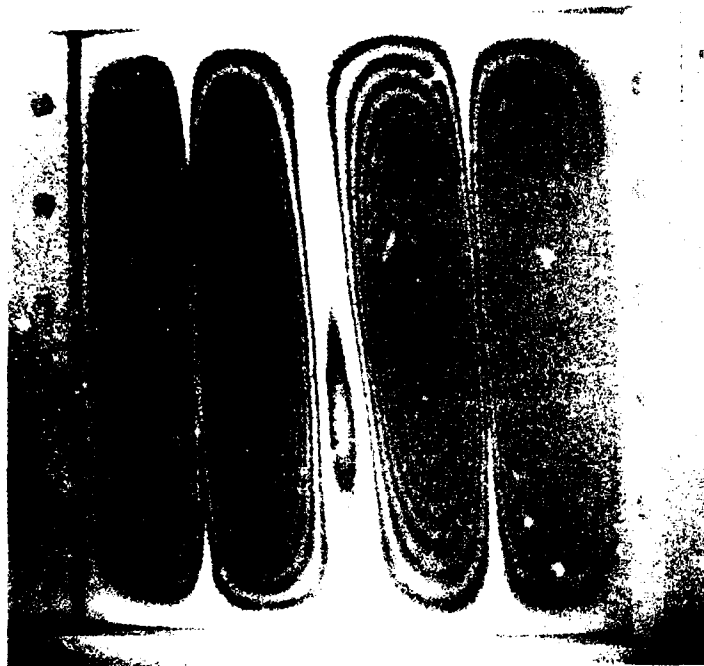Figure 16: Solid Panel Mode 3

51

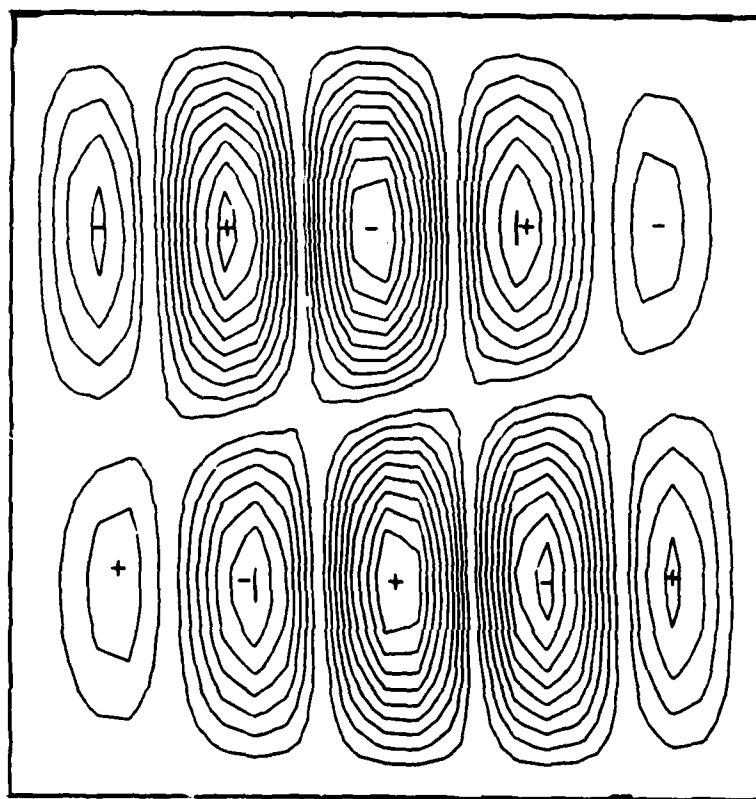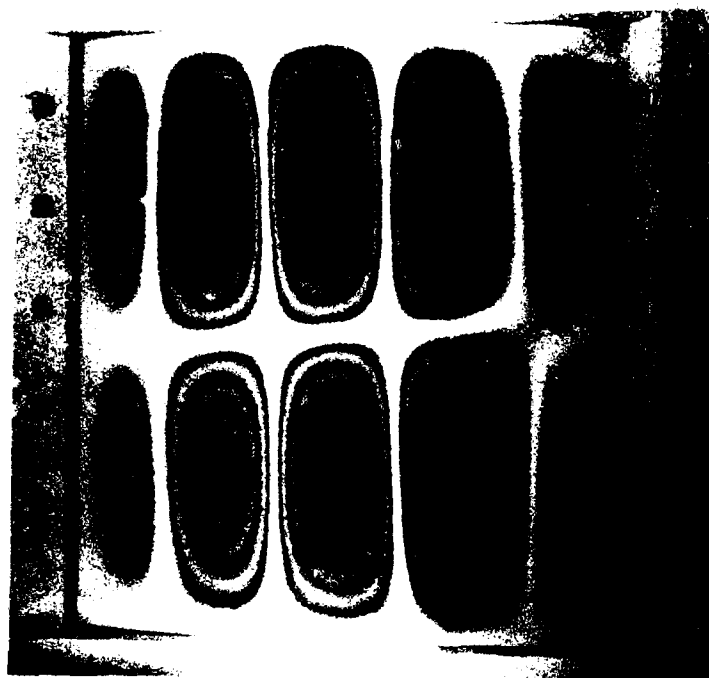Figure 17: Solid Panel Mode 4

52

Figure 18: Solid Panel Mode 5

53

panel. The first and second natural frequency on this panel were separated by approximately 7 percent of the highest frequency. The smearing exhibited between these two modes on the solid panel was not present on this panel. Additionally, the harmonics of the first symmetric mode (Mode 2) were as evident as on the solid panel. The symmetric mode clearly was similar on both panels with the level of displacement at a fixed sound level significantly greater than the antisymmetric modes. The experimental and numerical results are tabulated below.

2 × 2 CUTOUT

Mode Number	Frequency (Hz)		Percent Error
	STAGS	Experiment	
1	505	510	-1.0
2	527	546	-3.5
3	669	731 [**]	-8.5
4	691	705 [**]	-2.0
5	712	756	-5.8

Table 4

[**]Order Switch

54

As annotated, the order (as determined by the mode shape) of

modes 3 and 4 were reversed between the two methods.

However, the error values in Table 2 are computed using the

frequencies corresponding to identical eigenvectors (Fig 21,

22). The two frequencies of mode 3 and mode 4 differ by

less than 4 percent and the shift may be attributed to less

than perfect boundary conditions in the test fixture.

Problems with the clamping in mode 3 and 4 are visible in

the holograms. Note that the regions of displacement to the

right of the cutout do not descend to the bottom. Clamping

appears to be weak on the bottom clamp. Despite the shift,

the computed natural frequencies still exhibit good accuracy

for all five modes. The eigenvectors are compared in

Figures 19-23. Again, STAGS-C1 proved outstanding in

predicting mode shapes. When compared with the mode shapes

of the solid panel, the smallest cutout appears to have very

little effect for the first four modes. Similiarly, the

shift toward the upper left is evident in some modes.

Although mode 5 differs dramatically between the solid and

the 2 x 2 inch cutout panels the computer code was able to
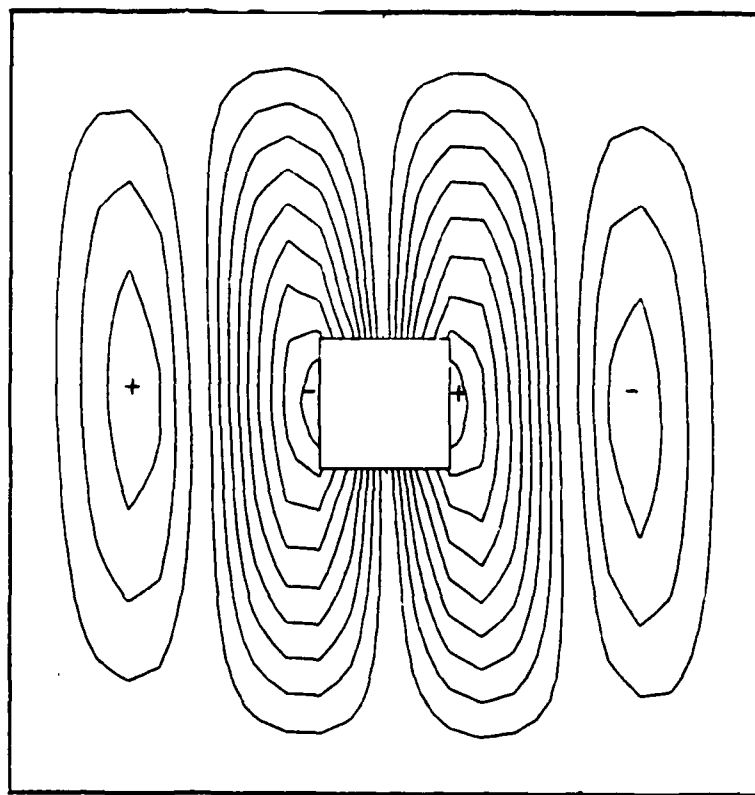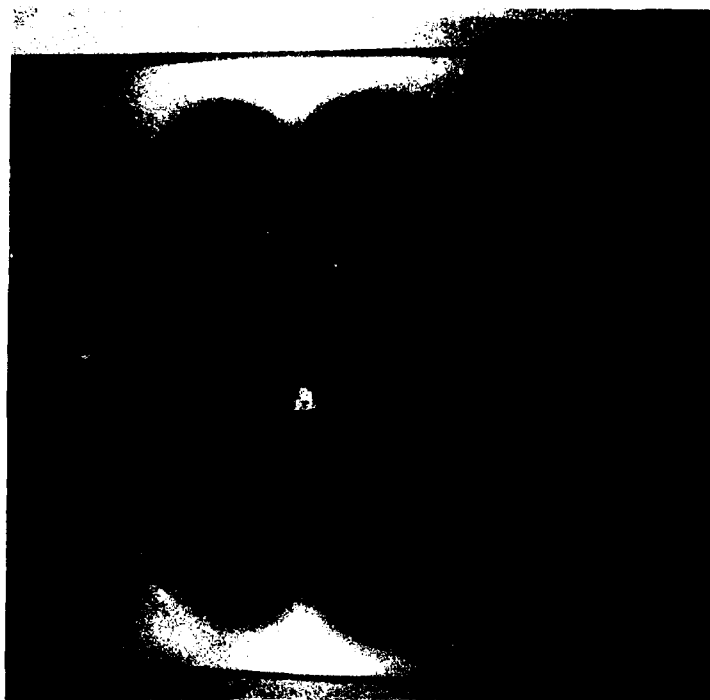
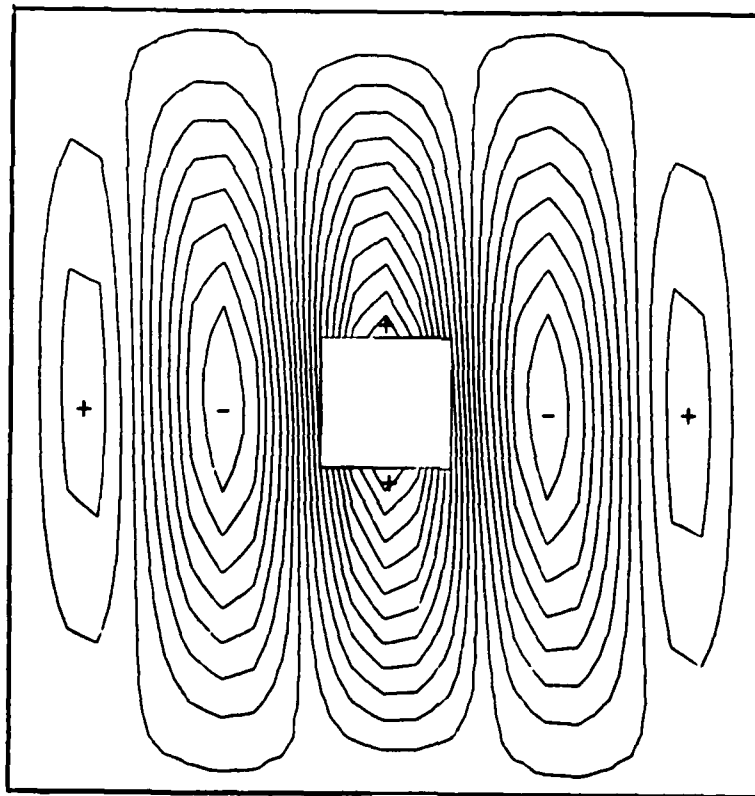accurately predict the change.

55

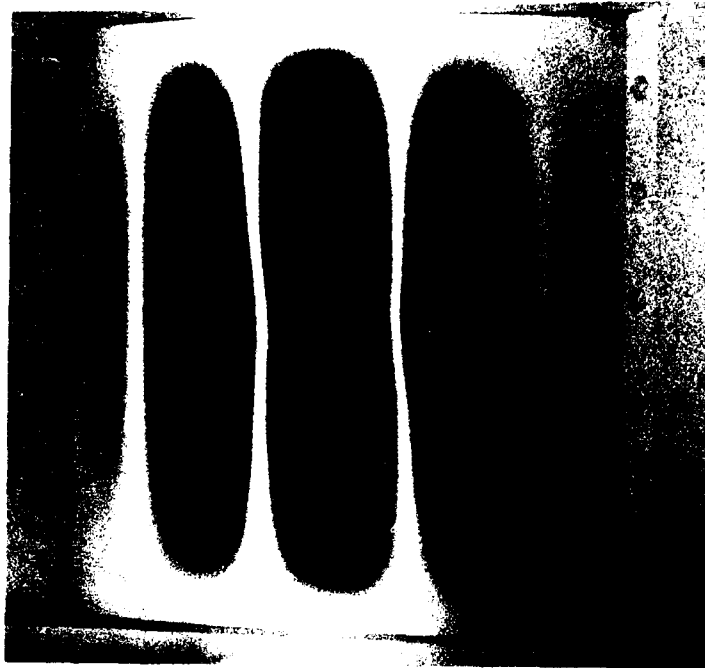Figure 19: 2 × 2 Inch Cutout Mode 1

Figure 20:   2 x 2 Inch Cutout Mode 2

57

Figure 21:   2 x 2 Inch Cutout Mode 3

Figure 22:   2 x 2 Inch Cutout Mode 4

Figure 23:   2 x 2 Inch Cutout Mode 5

The 2 x 4 Inch Cutout

The STAGS-C1 and holographic results are summarized in
Table 5.

2 × 4 CUTOUT

Mode	Frequency (Hz)		Percent
Number	STAGS	Experiment	Error
1	454	419	+7.7
2	536	463	+13.6
3	562	579	-2.9
4	631	670	-5.8
5	703	714	-1.5

Table 5

This panel was the only one that exhibited significant error
for the first two modes. Comparing the holograms and
contour plots does not identify a region where boundary
conditions are weak. It should be pointed out that for the
first two panels STAGS just slightly under-estimated the
natural frequencies of the first modes and had a tendency to

61

increasingly underestimate them at the higher ones. For the
2 x 4 cutout, the program overestimated the lower mode
natural frequencies. The trend toward an increasing
negative percentage error produced in this case the lowest
errors at the higher modes. Thus it appears that either
STAGS overestimated the panel stiffness or the clamped
boundary conditions were "soft" on all edges.

The mode shape estimations of STAGS were particularly
good for this panel. (Figs. 24-28) The tilting of the
antinode regions noted in previous panels is again evident.
Additionally, the bulging of the antinode region about the
cutout is apparent in the holograms and the numerical
results. The loss of stiffness at the center of the panel
is much more visible for this panel than the 2 x 2 inch
cutout. The deflected regions about the first symmetric
mode (2) extend into the cutout. The symmetric third mode
is the only one seen in any of the panels, while mode 4 and
5 appear remarkably similiar in shape to modes 3 and 5 of
the solid and 2 x 2 inch cutout panels. The failure of this
panel to follow the mode shape patterns exhibited by the
previous two was an indicator of the behavior found in the 4
x 4 inch cutout panel.
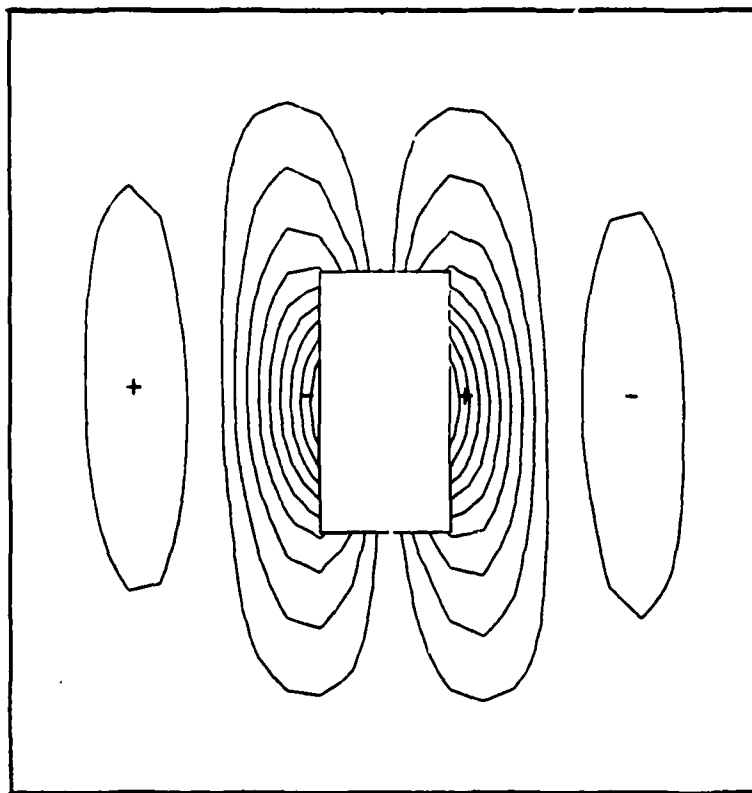
Figure 24: 2 x 4 Inch Cutout Mode 1
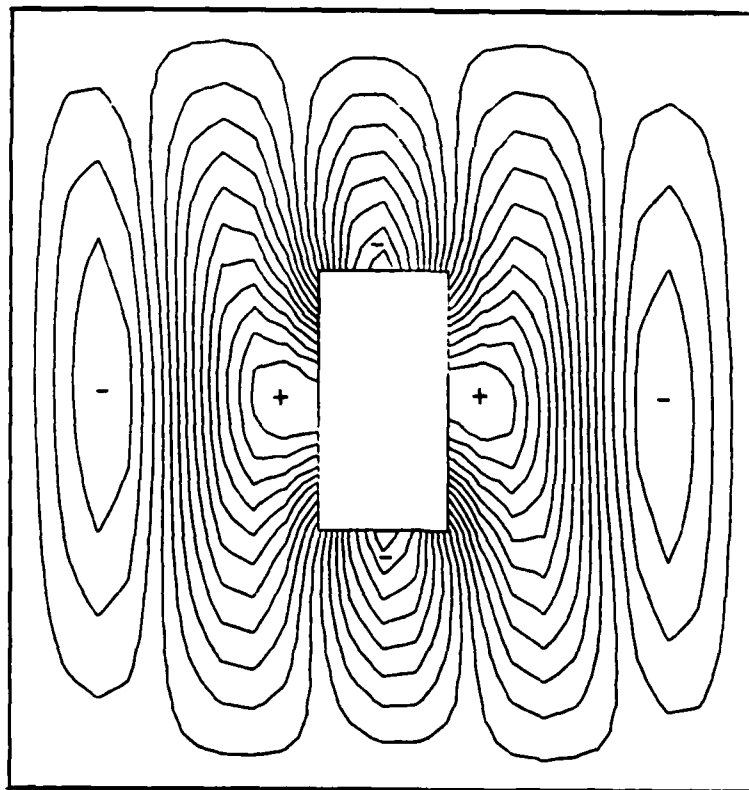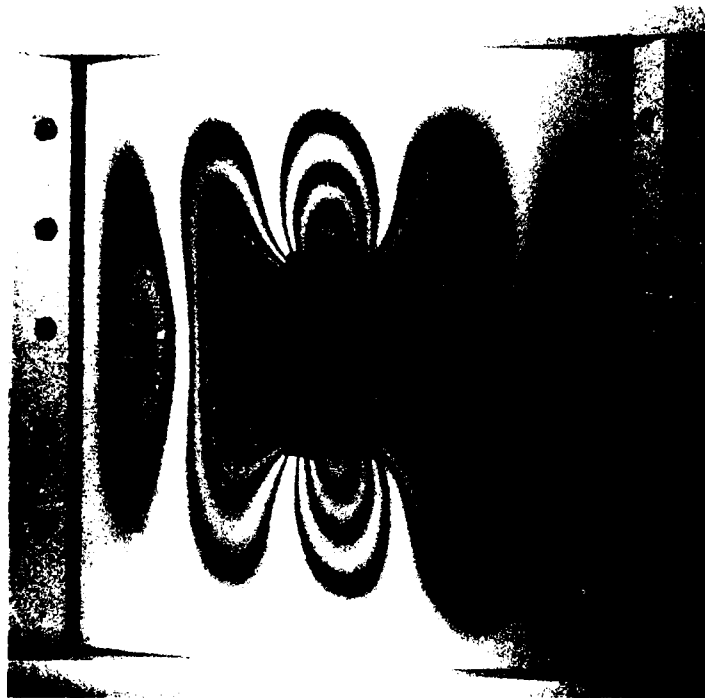
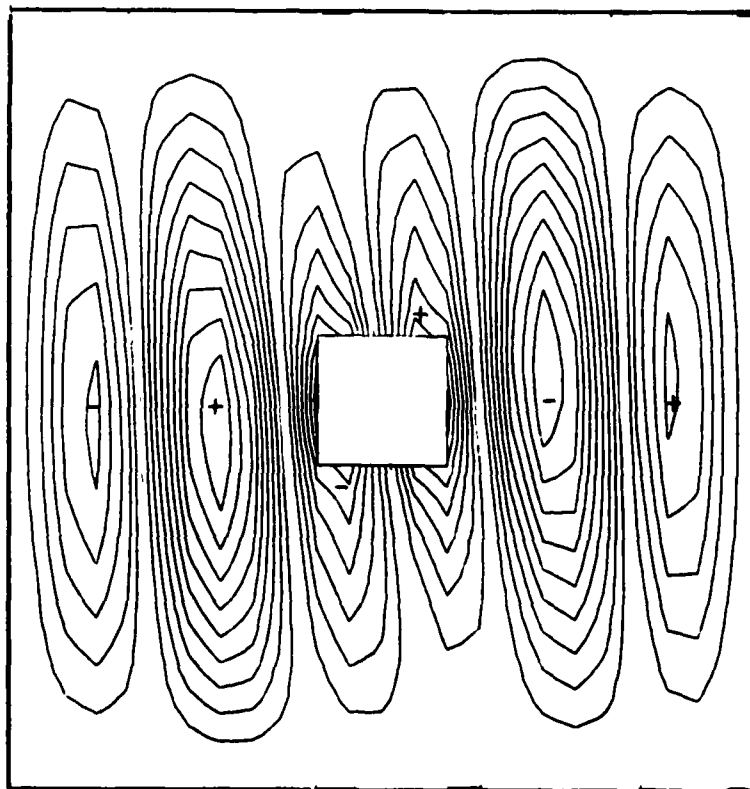Figure 25: 2 x 4 Inch Cutout Mode 2
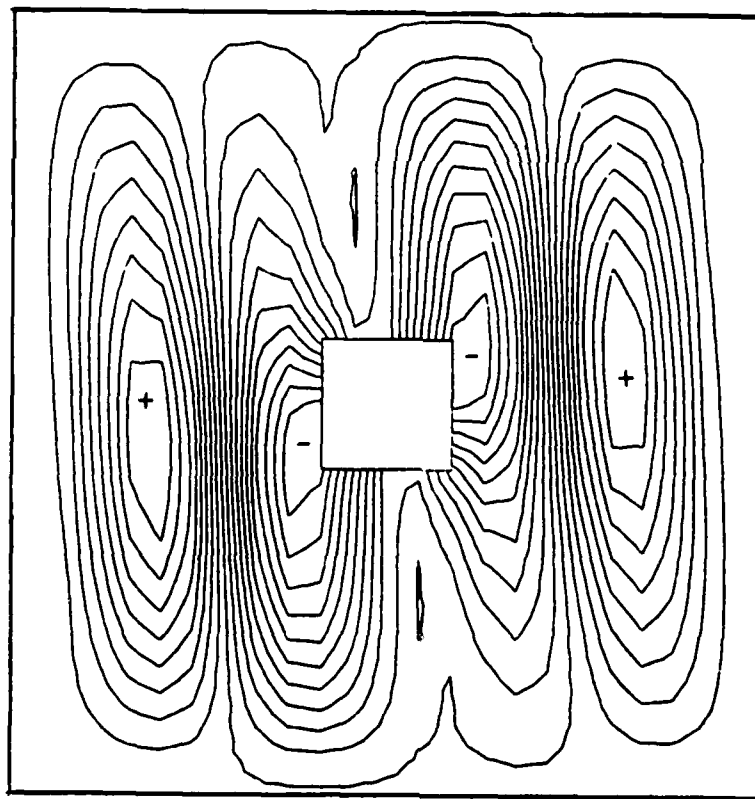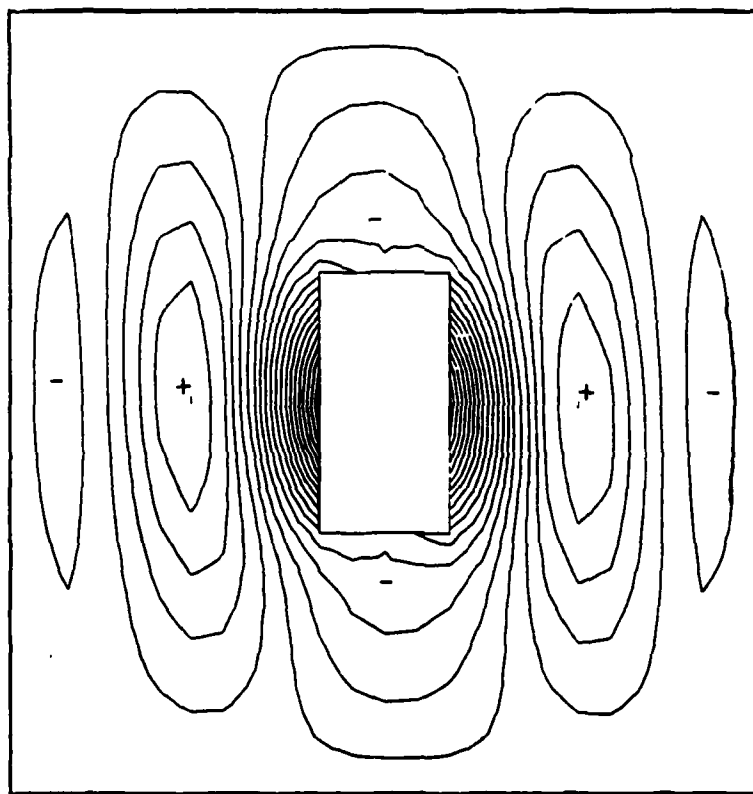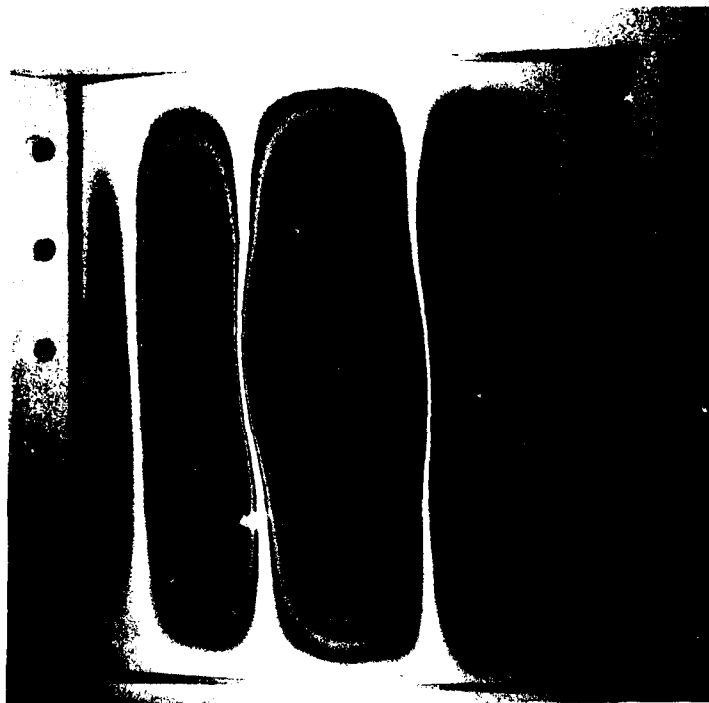
Figure 26:   2 x 4 Inch Cutout Mode 3

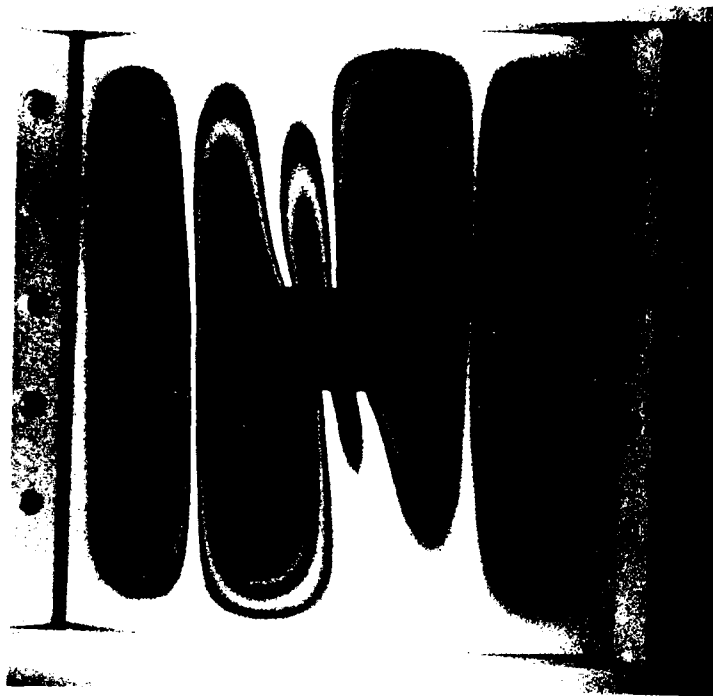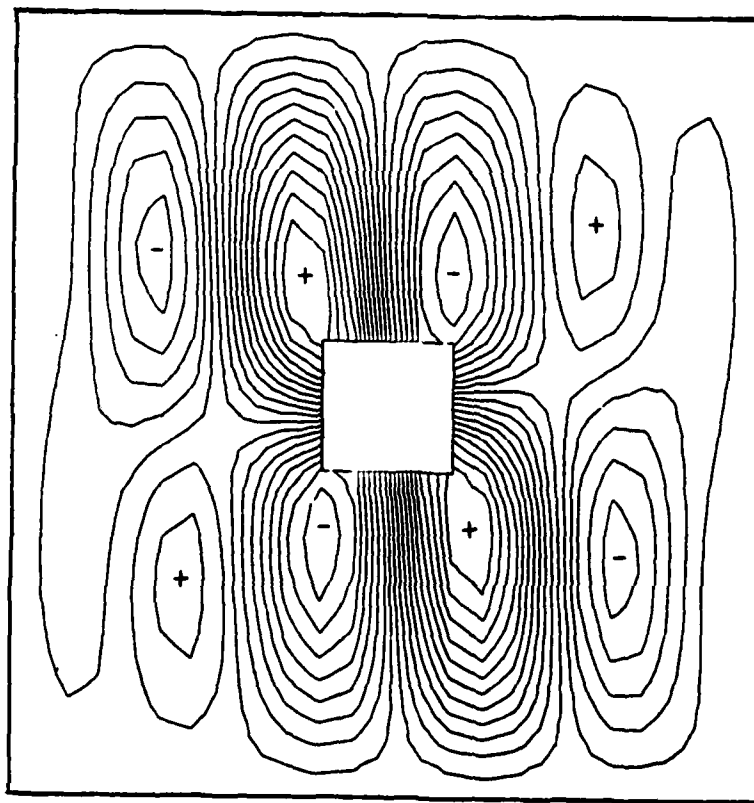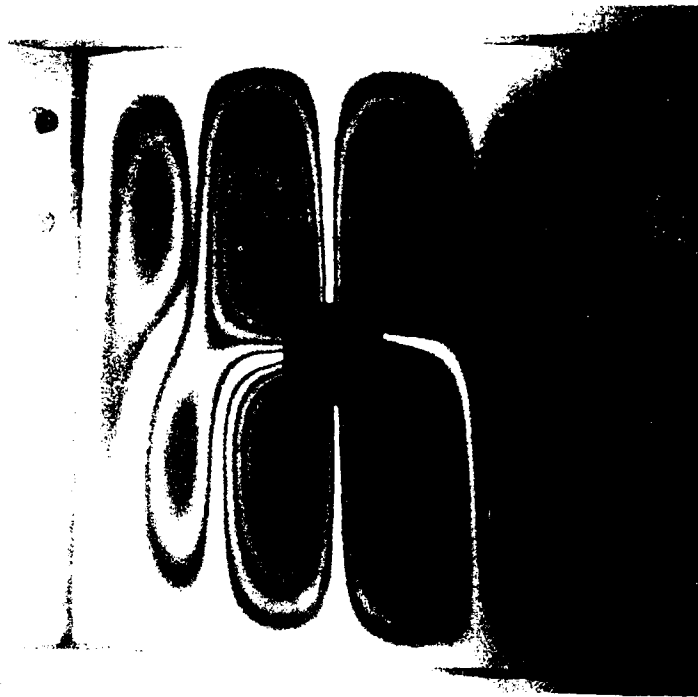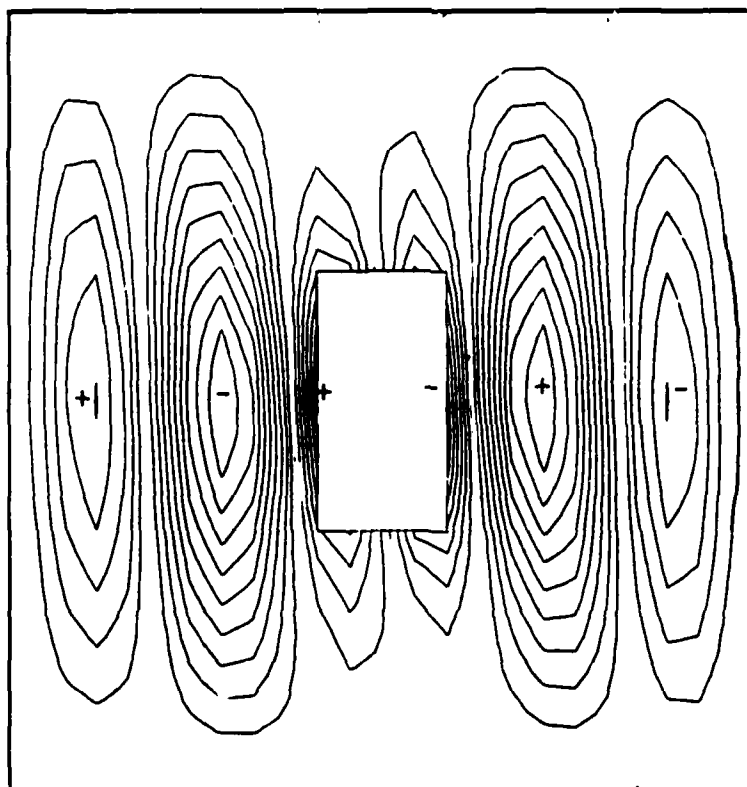Figure 27:   2 x 4 Inch Cutout Mode 4
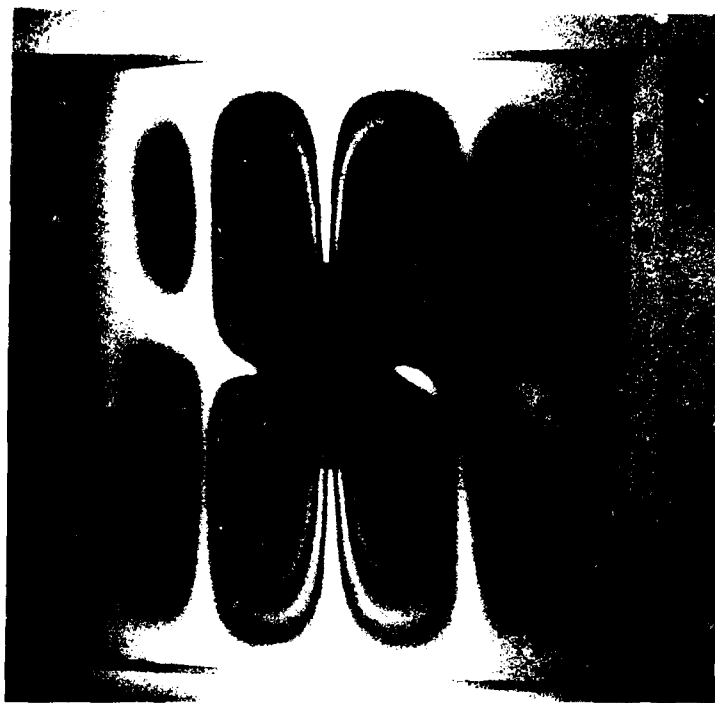
Figure 28: 2 x 4 Inch Cutout Mode 5

67

The 4 x 4 Inch Cutout

The natural frequencies are tabulated in Table 6. It
is apparent that the STAGS results overestimate the first
two frequencies (though to a smaller degree) as it had for
the 2 x 4 inch cutout. Again, the trend toward increasing
underestimation of higher modes is indicated. Despite these
observations, the overall level of accuracy is still quite
good. It should be noted that the 4 x 4 inch cutout
represents approximately 11 percent of the surface area.

4 x 4 CUTOUT

Mode	Frequency (Hz)		Percent
Number	STAGS	Experiment	Error
1	485	477	+1.6
2	514	510[*]	+0.7
3	612	618	-1.0
4	644	691	-6.8
5	689	748	-7.9

Table 6

This reduction in area precipitated a 9 percent decrease in natural frequency for the experimental results. However, the first mode shape for this cutout is symmetric and the second mode shape is antisymmetric. This is a reversal of the behavior exhibited in the first three panels. The finite element model was again accurate in predicting this behavior.

Locating the second natural frequency for this cutout proved quite difficult. When scanning through the frequency range the mode shapes 1, 3, 4, and 5, as predicted by STAGS, were quickly located using the two horn excitation arrangement. The accuracy of STAGS in predicting natural frequencies and in particular the mode shapes of the first three panels indicated that perhaps the previous procedures has missed a mode. In order to increase the intensity of the excitation, one of the two horns was moved to the front surface. After rewiring to return the horns to in-phase motion, the experiment was again repeated. The mode shape seen in Fig 30 (note: horn in photo) is the response seen at 510 Hz. This mode shape does not exhibit the correlation seen at modes 1, 3, 4, and 5 but was definitely present. To preclude this response as being a harmonic, the optical probe was employed. The large displacement patterns seen in Fig 30 are indeed oscillating at 510 Hz. It proved

impossible to eliminate all motion along the free edge at
this frequency. While the information achieved through use
of the optical probe and the holograms were not conclusive,
the transition to the mode shape seen in the photograph
indicated an attempt by the panel to assume a mode shape.
It is strongly felt that a natural frequency does indeed
exist at 510 Hz and that the correct combination of boundary
conditions and excitation was never found to illicit the
response predicted by STAGS. All other mode shapes in this
panel were predicted with accuracy found in other panels.
Mode 3 and 5 (Fig 31 and 33) indicate some looseness in the
bottom clamp. Overall, the results for this panel as with
the others shows a close correlation between the finite
element and experimental techniques.
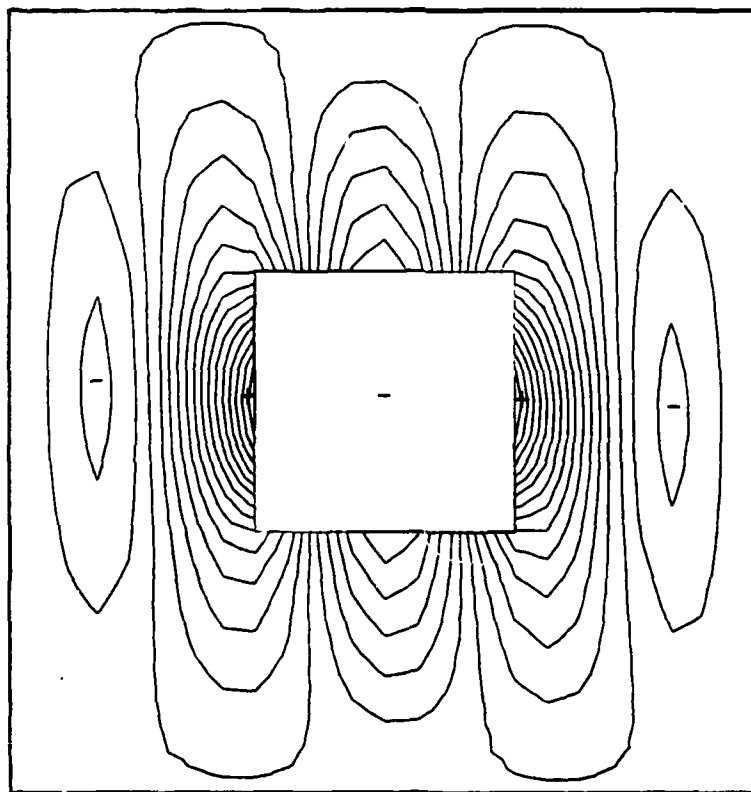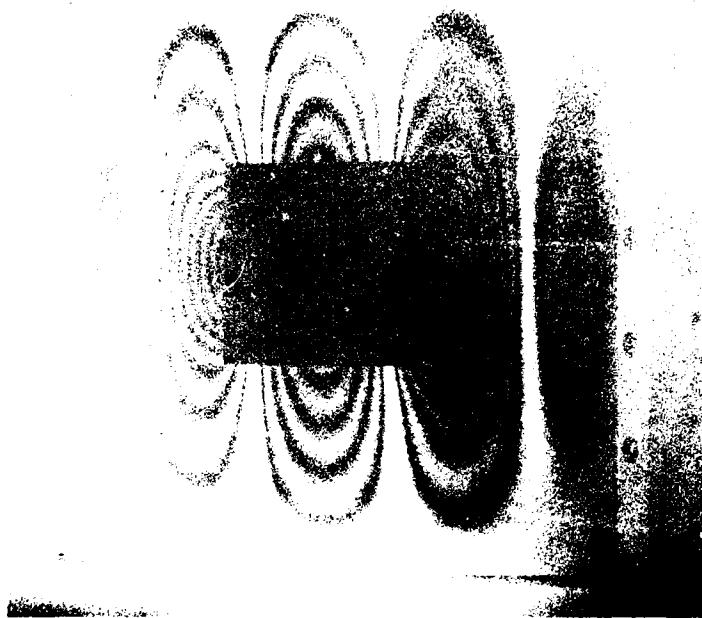
Figure 29: 4 x 4 Inch Cutout Mode 1

71
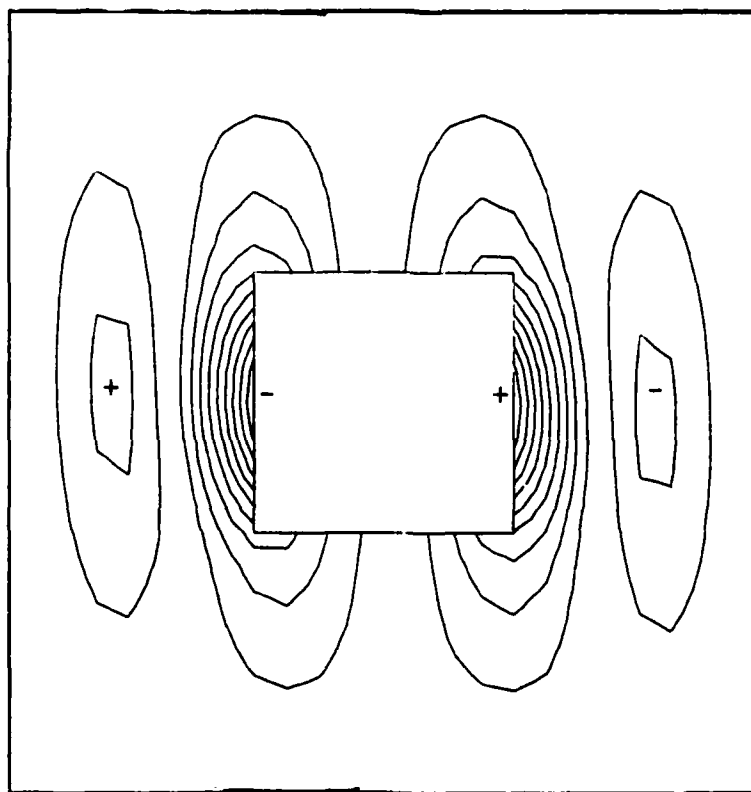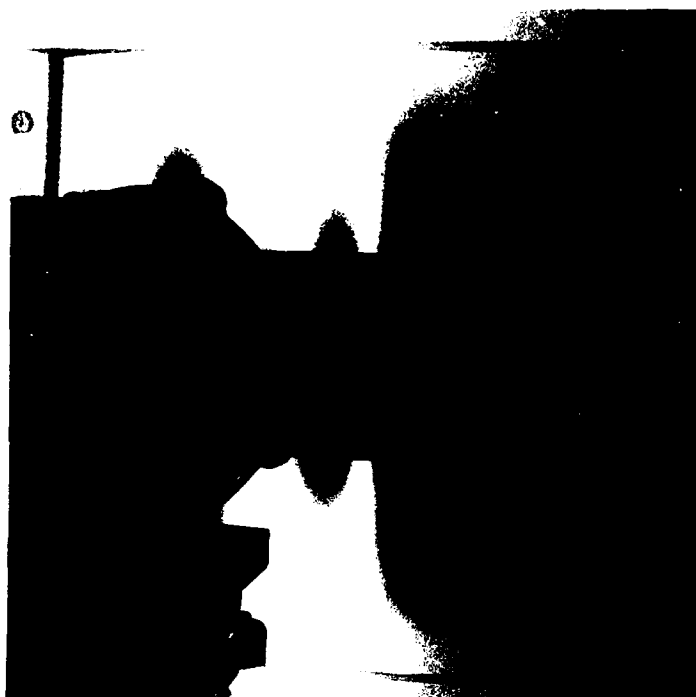
Figure 30:   4 x 4 Inch Cutout Mode 2

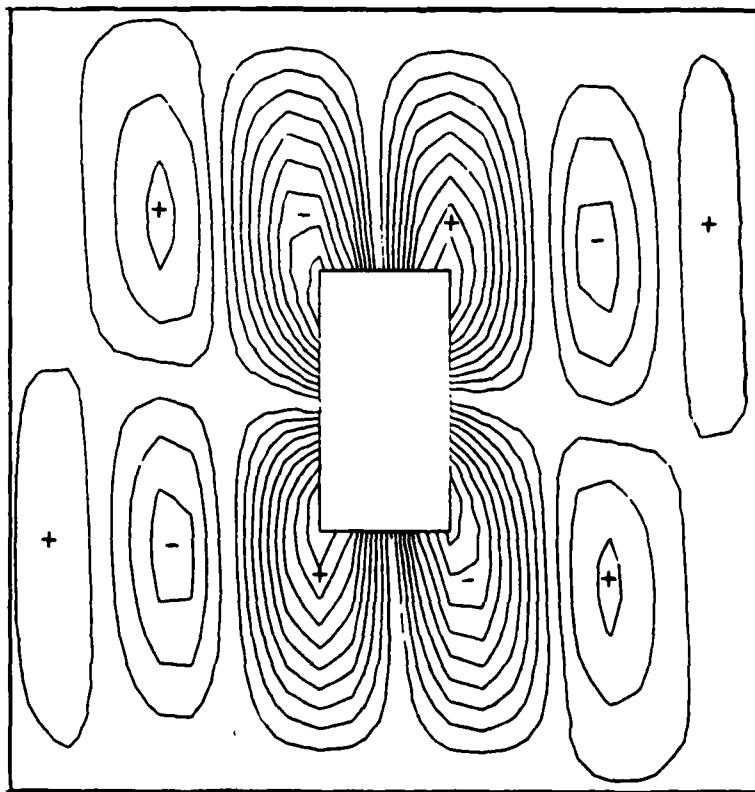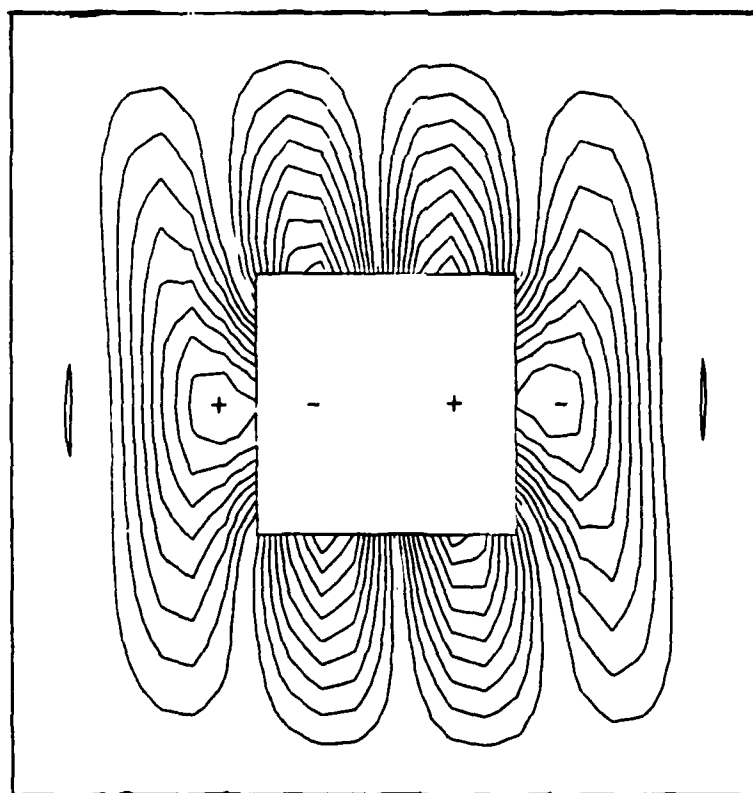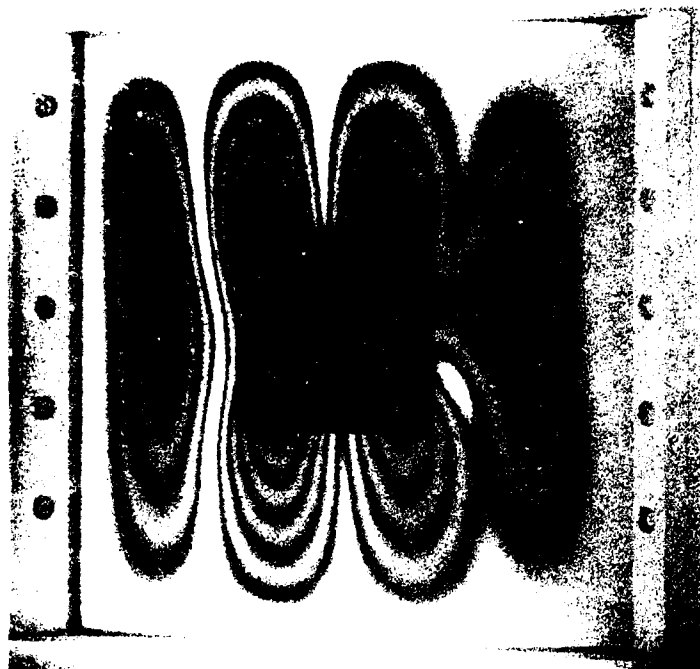Figure 31: 4 × 4 Inch Cutout Mode 3
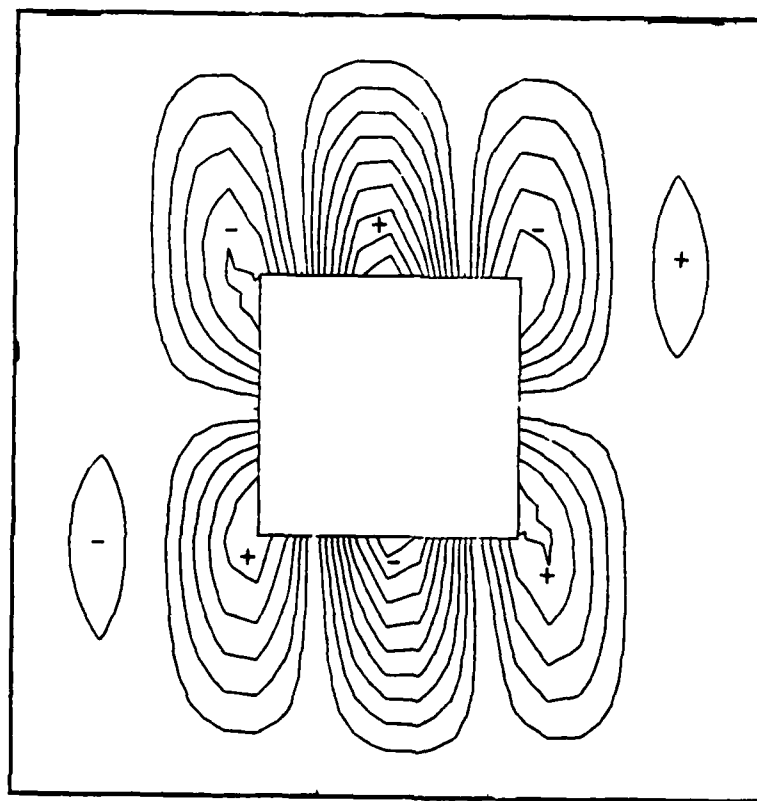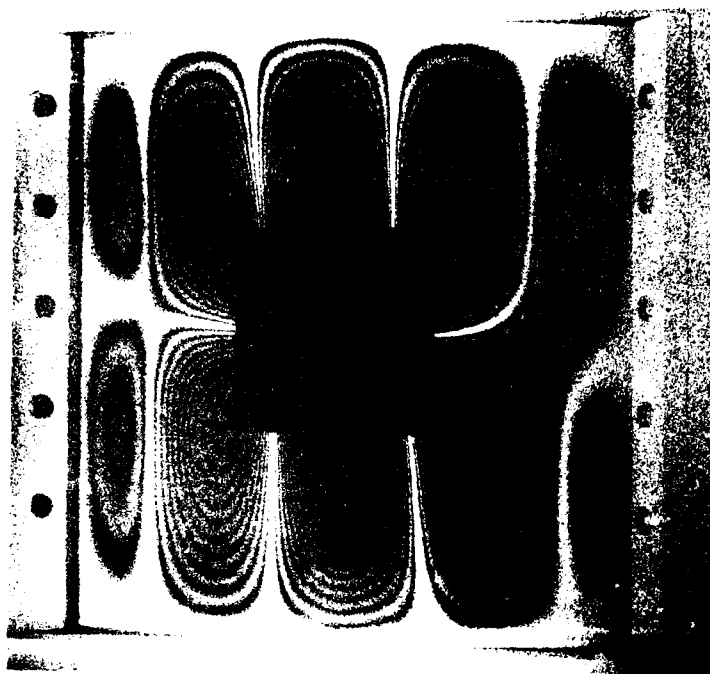
Figure 32:   4 × 4 Inch Cutout Mode 4
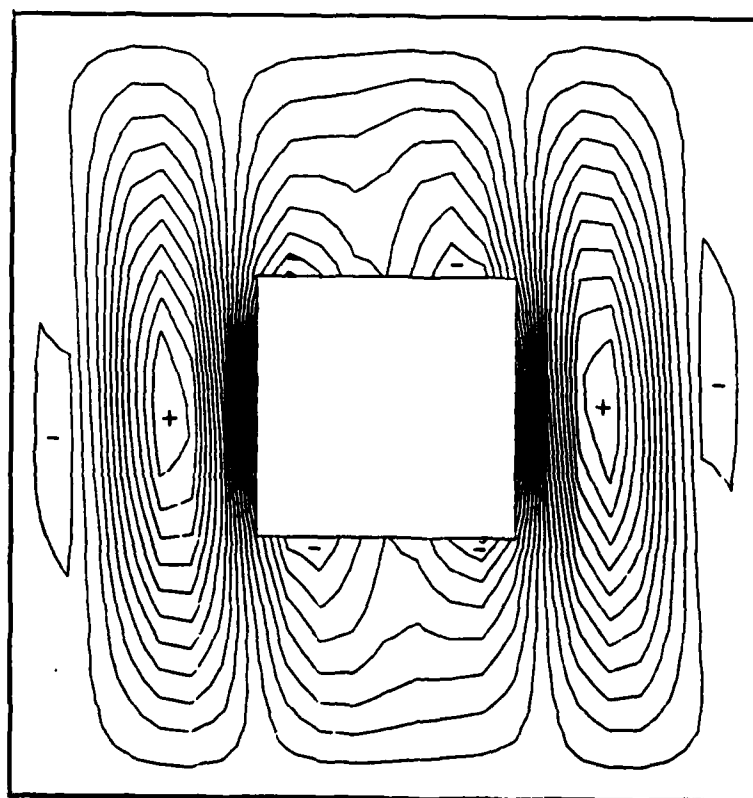
Figure 33: 4 x 4 Inch Cutout Mode 5

Cutout Effects

As seen in the previous discussion, the boundary
conditions generated by the test fixture had a significant
effect on the mode shapes. As seen in Figure 21 the loss of
clamping at the bottom of test fixture resulted in failure
of the displacement pattern to extend to the bottom of the
panel. Given the narrow range of frequencies involved and
the closeness of some of the natural frequencies, a small
deviation from the exact value due to inexact boundary
conditions would represent a significant deviation. This
deviation would effectively mask any trends or conclusions
based on experimental values. Thus, the close correlation
of the experimentally determined data (frequencies and mode
shapes) with that of numerically derived, supported the use
of the numerical values to analyze the effects of cutouts.
This conclusion is further supported in that an analysis
based on the numerical results would be the results based on
mathematically perfect clamped boundary conditions. Figure
34 is a plot of natural frequencies generated by STAGS C-1
for each of the four panels. Although there are a limited
number of data points this plot clearly shows a trend toward
lower frequencies (particularly for the highest three modes)
when cutouts are added. Figure 35 graphically displays the

effect of mass removal on each mode. Note that this is a

comparison of the modes as they occurred in the numerical

sequence. Mode 3 for the 2 x 4 inch cutout is not the same

shape as Mode 3 of the 2 x 2 inch panel; both simply are the

third from the lowest frequency for each panel respectively.

If in a simplified analysis the panels are modelled as a

single degree of freedom system, then:

$$\omega = \sqrt{\frac{K}{M}} \qquad\qquad (42)$$

where   K = stiffness

             M = Mass.

Then the apparent decrease in frequency (Fig 35) for the

2 x 2 inch cutouts suggests a decrease in stiffness versus

mass. Similiarly, the increase in frequency for the modes

1, 3, and 4 for the 4 x 4 cutout implies mass is decreasing

faster than stiffness. Although the data points are limited

in number, the trend may indicate that material removal

along the vertical plane of symmetry is dominant for panel

stiffness.

Referencing Figures 47,48,54,55,61,62,69,and 70 an

apparent shift in symmetry occured for the first and second

mode shapes of the 4 x 4 inch cutout panel. While this

result was unexpected, it was also observed experimentally.

77

To further explore this event, additional finite element runs with the same material properties were completed for a 3 x 3 and 3.6 x 3.6 inch cutout. The results were are shown on Fig. 35. The 3 x 3 inch hole retained the symmetry seen in the smaller cutouts while the larger 3.6 x 3.6 inch cutout displayed the symmetry shift seen in the 4 x 4 inch cutout. Additional runs were then accomplished in order to explore the contribution of material properties to this apparent shift in symmetry. While the original geometry of the panel was retained, the orthotropic material was replaced with an isotropic material with a modulus of elasticity equivalent to E_1. The symmetry shift was again evident for the 4 x 4 inch cutout. Thus, if the symmetry shift is indeed real it appears to be a function of the panel radius and cutout size.

In conclusion, the effects of the interior cutouts tends to create a moderate decrease in natural frequency for this panel geometry and material properties. The geometry of the problem analyzed in this case appears to significantly alter the mode shapes of the panels. This observation is contrary to that found for flat plates [12]. Clearly, additional analysis of the effects of curvature on composite materials is required.

78
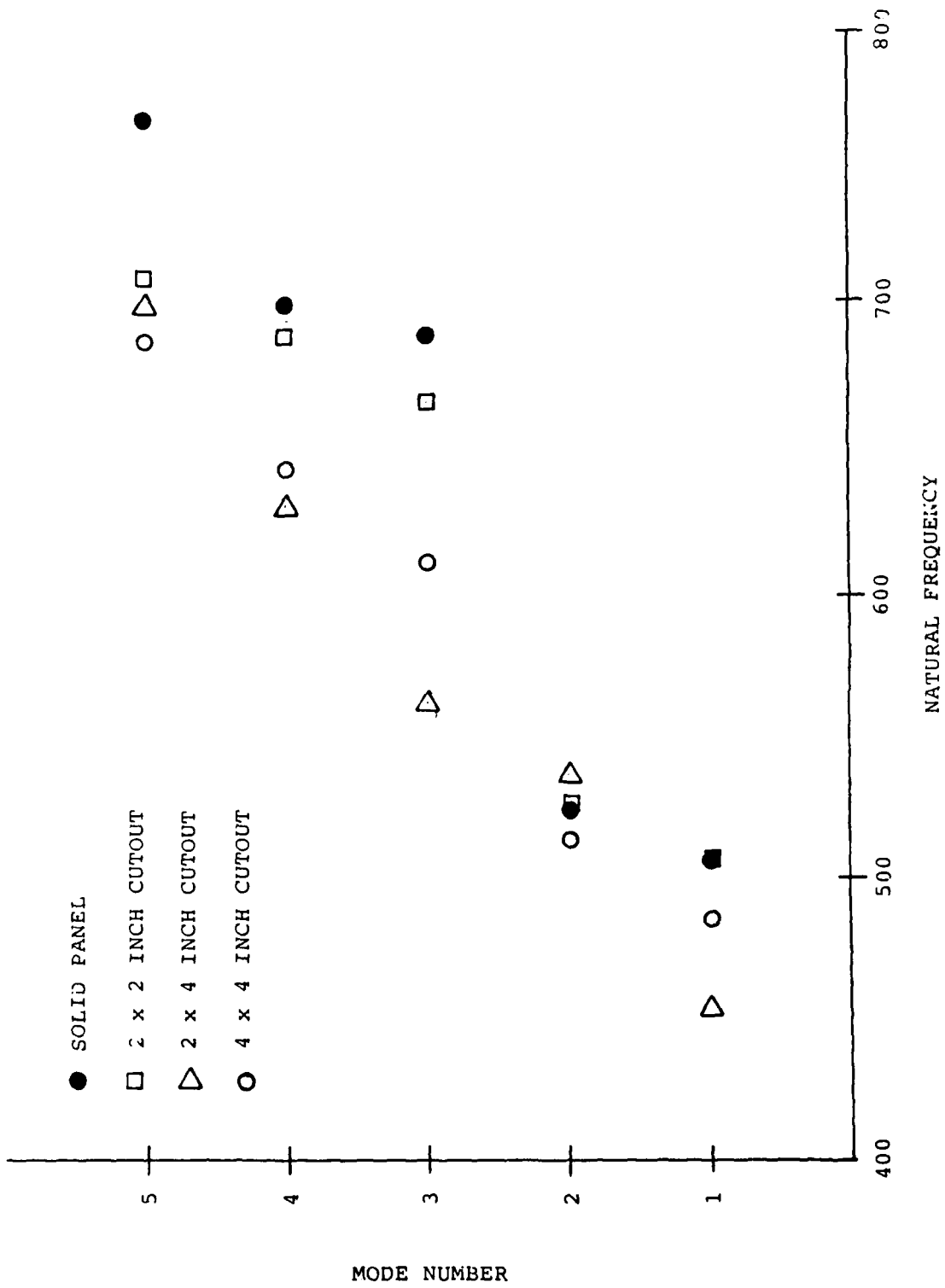
Figure 34: Panel Natural Frequencies
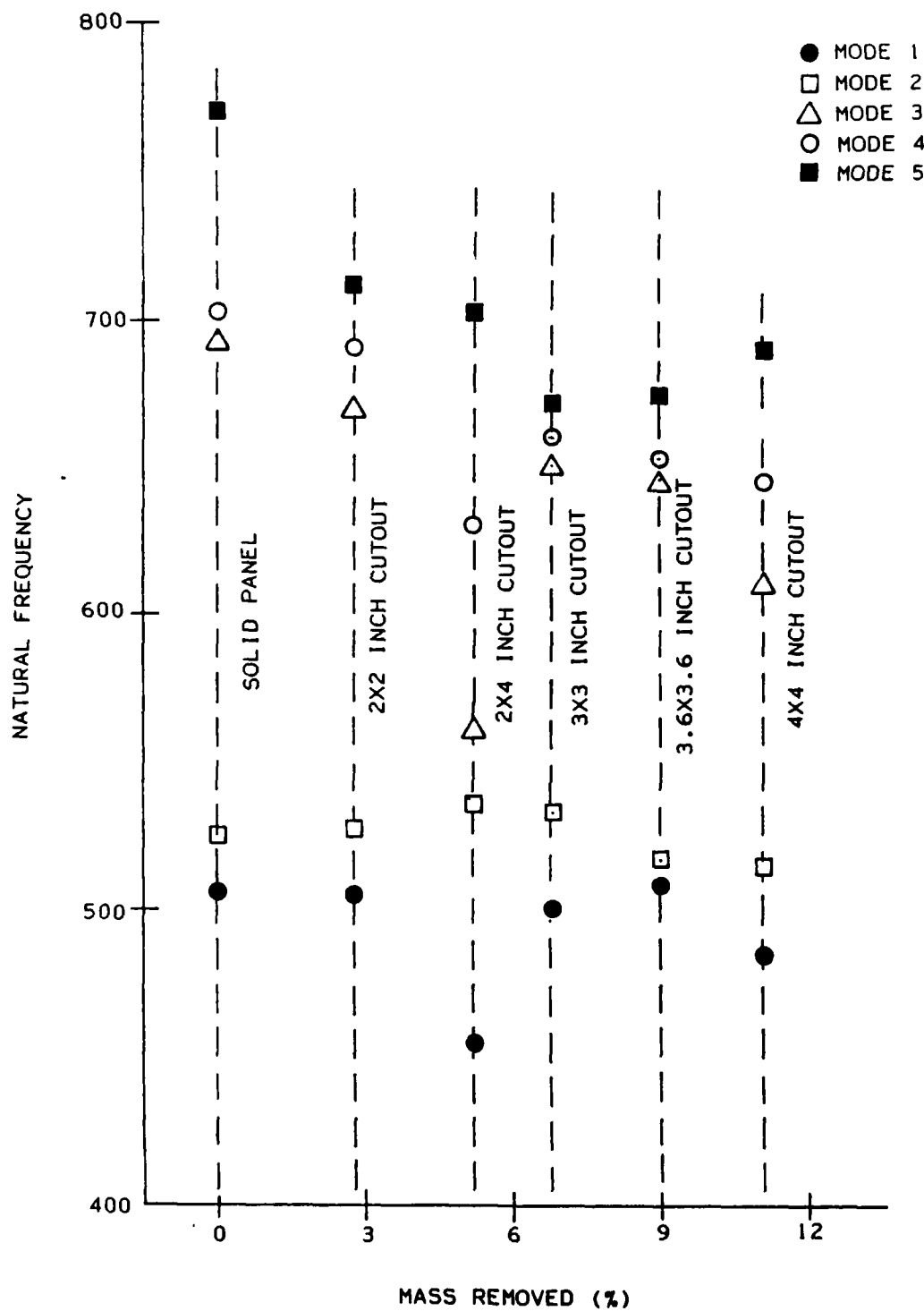
Figure 35:   Effects of Mass Removal

VII. CONCLUSIONS

In addition to the observations and conclusions in previous chapters, the following additional conclusions are included:

1.   The STAGS C-1 computer code, assuming small displacements and linear stress-strain relationships, proved excellent at predicting the mode shapes of the composite panels tested here.

2.   Similiarly, the STAGS C-1 code proved capable of predicting natural frequencies within limits of engineering accuracy.

3. For the clamped-clamped boundary conditions, the QUAF 410 plate element proved as effective as the higher order QUAF 411 element.

4.   For the smallest cutout, the mode shapes change very little in comparison with the solid panel.

5. Natural frequencies tend to decrease with cutout size.

6. Mode shapes for the larger cutouts are significantly altered. The inclusion of mode shapes not found in the solid panel as well as symmetry shifts in fundamental modes were observed for increasing cutout size.

VIII.   RECOMMENDATIONS

1.   Using both finite element analysis and holographic
interferometry, the range at this study should be extended
to higher frequencies and mode shapes.   Similiarly, the
study on nonsymmetric laminates should be included.
Verifying the accuracy of the finite element code to model
the coupling of bending and extensional stresses should
extend confidence in the code for these type of laminates.

2.   Interchanging the order of the 45 degree lamina should
prove instructional on their effect on the left tilt seen in
the displacement patterns.

3.   The analytical techniques used in this study should be
extended to other boundary conditions.

BIBLIOGRAPHY

1. Almroth, B. O., Brogan, F. A., and Stanley, G. M.
    STAGS THEORY MANUAL, Cosmic Program No. HQN-10960.
    Applied Mechanics Laboratory, Lockheed Palo Alto
    Research Laboratory, April 1983.

2. Janaise, Thomas C.   A Parametric Study of Surface
    Imperfections and Small Cutouts in a Composite Panel.
    Master's Thesis, GAE/AA/82D-15.   School of Engineering,
    Air Force Institute of Technology (AU), Wright-
    Patterson AFB, OH, December 1982.

3. Jones, Robert M.   Mechanics of Composite Materials.
    Washington DC: Scripta Book Company, 1975.

4. Cook, Robert D.   Concepts and Applications of Finite
    Element Analysis (Second Addition).   New York: John
    Wiley and Sons, Inc., 1981.

5. Erf, Robert K.   Holographic Nondestructive Testing   New
    York: Academic Press, Inc., 1974

6. Almroth, B. O., Brogan, F. A., and Stanley, G. M.
    Structural Analysis of General Shells Volume II User
    Instructions for STAGS-C1.   LMSC-D633837.   Applied
    Mechanics Laboratory, Lockheed Palo Alto Research
    Laboratory, January 1981.

7. Meirovitch, Leonard.   Elements of Vibration Analaysis.
    New York: McGraw-Hill Book Company, 1975.

8. Almroth, B. O. and Brogan, F. R.   Numerical Procedures
    for Analysis of Structural Shells.   AFWAL-TR-80-3129.
    Wright-Patterson AFB, Ohio: Air Force Wright
    Aeronautical Laboratory, March 1981.

9. Ashton, J. E. and J. M. Whitney.   Theory of Laminated
    Plates.   Westport, Conn: Technomic Publishing Co,
    1970.

10. Raju, P. N.   "Vibration of Annular Plates", Journal of
    the Aeronautical Society of India,   14: 37-52   (May
    1962).

END

FILMED

DTIC
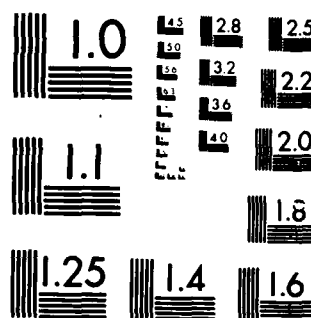
MICROCOPY RESOLUTION TEST CHART

NATIONAL BUREAU OF STANDARDS-1963-A

11. Jones, Robert M. and Harold S. Morgan. "Buckling and Vibration of Cross-Ply Laminated Circular Cylindrical Shells", AIAA Paper No. 74-33, 12th Aerospace Science Meeting, Washington DC, 30 January - 1 February 1974.

12. Monahan, Jon. Natural Frequencies and Mode Shapes of Plates with Interior Cutouts. Master's Thesis, GAM/MC/71-1. School of Engineering. Air Force Institute of Technology (AU), Wright-Patterson AFB, Ohio, September 1970.

13. Knight, Norman F., Jr., Engineer. Telephone interview. NASA, Langley. 9 October 1985.

14. Mindle, Wayne L. The Multiple Mode Phenomenon in the Vibration of Curved Cantilevered Blades. AFIT-TR-EN-85-5. Wright-Patterson AFB, Ohio. Air Force Institute of Technology, September 1985.

15. Thomas, K. and Sobel, L. H. Evaluation of the STAGS C-1 Shell Analysis Program. WARD-10881. Madison PA: Westinghouse Advanced Reactors Division, August 1981.

16. Kock, Winston E. Lasers and Holography, AnIntroduction to Coherent Optics, New York: Dover Publications, Inc., 1981.

```
SAMPLE INPUT FILE 2X4 INCH CUTOUT 410 ELMT   $A1
2,0,1,0,0,0,0,0,0                  $B1 SMALL VIBRATIONS,SAVE
                                       MODEL DATA,GRID TEST
1,0,0                              $B2 ONE SHELL
1,0,1,0                            $B3 SINGLE MATERIAL,ONE
                                       WALL TYPE
1                                  $C1
1,0,7000,1                         $D2 7000 CPU SECONDS
5,0,0,0                            $D3 EIGENVALUES,SHIFT,UPPER
                                       LOWER BOUNDS
25,25                              $F1 ROWS,COLUMNS
1,0                                $I1
18.84E06,.021813,.9099E06,.055,.0216216,1.468E06,15.2 $I2
                                       MATERIAL PROPERTIES
1,1,8                              $K1 GENERAL LAYERED WALL-
                                       EIGHT LAYERS
1,.005,0.,0                        $K2 PLY THICKNESS - FIBER
                                       ANGLE
1,.005,-45.,0                      $K2
1,.005,45.,0                       $K2
1,.005,90.,0                       $K2
1,.005,90.,0                       $K2
1,.005,45.,0                       $K2
1,.005,-45.,0                      $K2
1,.005,0.,0                        $K2
5,0                                $M1 CYLINDER LOCAL
                                       COORDINATES COINCIDE
                                       WITH GLOBAL
0.0,12.0,-28.648,28.648,12.        $M2A
X1,X2,Y1,Y2(DEGREES),RADIUS
1,0                                $M5 NO IMPERFECTIONS
410,0,0,1,0,0,0                    $N1 410 ELEMENT 25 X 25
                                       GRID
11,15,11,15                        $N4 CUTOUT DEFINITION
2,2,2,2                            $P1 CLAMPED ALL EDGES
0                                  $Q1
1                                  $R1 PRINT OUT DISPLACEMENTS
```

```
SAMPLE INPUT FILE SOLID PANEL 410 ELMT  $A1
2,0,1,0,0,0,0,0,0                         $B1 SMALL VIBRATIONS,SAVE
                                              MODEL DATA,GRID TEST
1,0,0                                     $B2 ONE SHELL
1,0,1,0                                   $B3 SINGLE MATERIAL,ONE
                                              WALL TYPE
1                                         $C1
1,0,7000,1                                $D2 7000 CPU SECONDS
5,0,0,0                                    $D3 EIGENVALUES,SHIFT,UPPER
                                              LOWER BOUNDS
25,25                                     $F1 ROWS,COLUMNS
1,0                                        $I1
18.84E06,.021813,.9099E06,.055,.0216216,1.468E06,15.2 $I2
                                              MATERIAL PROPERTIES
1,1,8                                     $K1 GENERAL LAYERED WALL-
                                              EIGHT LAYERS
1,.005,0.,0                               $K2 PLY THICKNESS - FIBER
                                              ANGLE
1,.005,-45.,0                             $K2
1,.005,45.,0                              $K2
1,.005,90.,0                              $K2
1,.005,90.,0                              $K2
1,.005,45.,0                              $K2
1,.005,-45.,0                             $K2
1,.005,0.,0                               $K2
5,0                                        $M1 CYLINDER LOCAL
                                              COORDINATES COINCIDE
                                              WITH GLOBAL
0.0,12.0,-28.648,28.648,12.              $M2A
X1,X2,Y1,Y2(DEGREES),RADIUS
1,0                                        $M5 NO IMPERFECTIONS
410,0,0,0,0,0,0                            $N1 410 ELEMENT 25 X 25
                                              GRID
2,2,2,2                                    $P1 CLAMPED ALL EDGES
0                                          $Q1
1                                          $R1 PRINT OUT DISPLACEMENTS
```

AIR ------

PART _____

P. O. Rimec.

AUTOCLAVE CYCLE B-240-T, REV A.

TIME, MINUTES
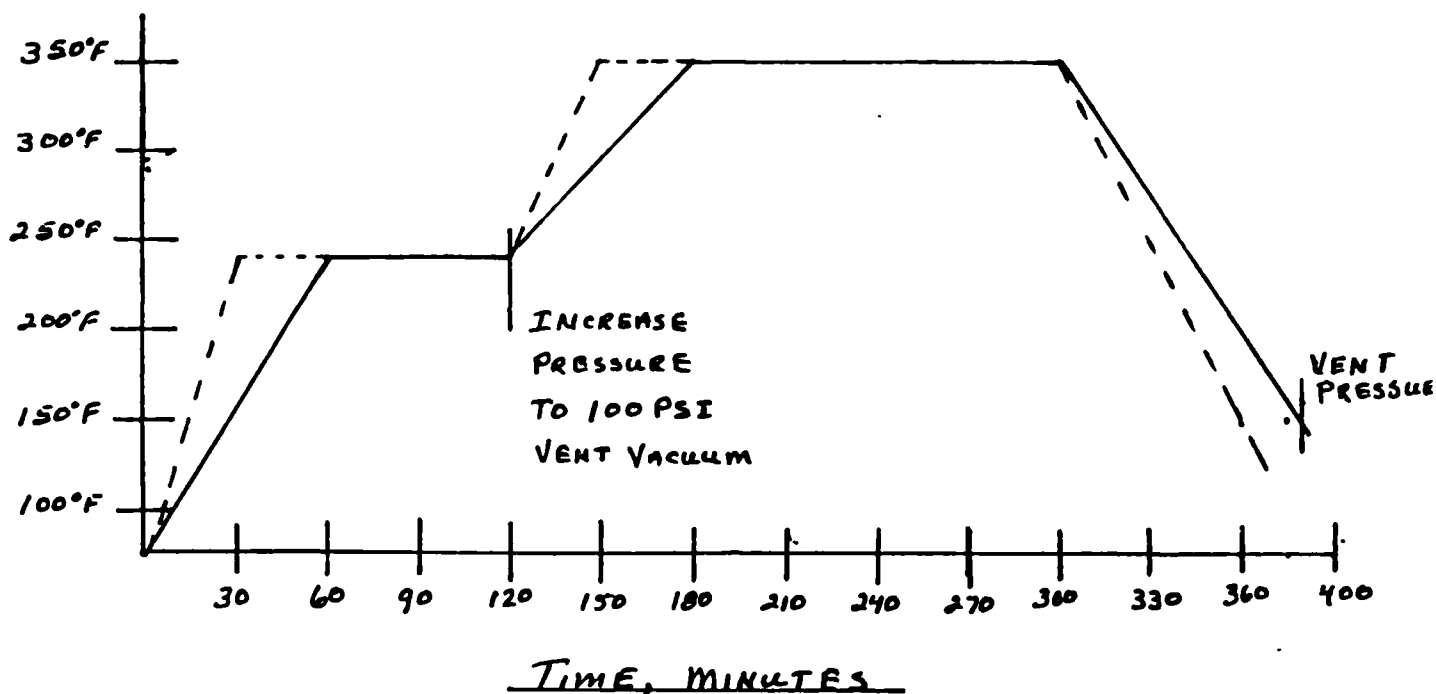
1. APPLY FULL VACUUM, 25 IN. Hg. MIN AND 85 PSI.

2. HEAT AIR TO 240°F IN 30±5 MIN. USING 90 KW HEATERS.

3. HOLD PART AT 240°F±5°F FOR 60 MINUTES UNDER
   85 PSI AND FULL VACUUM.

4. INCREASE PRESSURE TO 100 PSI AND VENT VACUUM.

5. HEAT AIR TO 350°F IN 30±5 MIN USING 90 KW HEATERS

6. HOLD PART AT 350±5°F AND 100PSI FOR 120 MINUTES.

7. APPLY FULL COOLING WATER AND COOL PART BELOW
   150°F IN LESS THAN 120 MIN.

8. WHEN PART IS BELOW 150°F, VENT PRESSURE.

88

VITA

Richard A. Walley was born on 15 October 1956 in Mobile, Alabama. He graduated from Mobile County High School in 1975 and attended the United States Air Force Academy from which he graduated in 1979 with a B.S. in Engineering Mechanics. He was commissioned as a Second Lieutenant in the USAF and assigned as a project engineer for the Air Force Armament Laboratory, Eglin AFB, FL. Projects included interior ballistics studies, telescoped ammunition gun design, the rapid fire light gas and electromagnetic gun design programs. He was then assigned to the Advanced Medium Range Air-to-Air Missile (AMRAAM) System Program Office as the executive officer. He entered the School of Engineering, Air Force Institute of Technology in June 1984.

REPORT DOCUMENTATION PAGE

1a. REPORT SECURITY CLASSIFICATION UNCLASSIFIED		1b. RESTRICTIVE MARKINGS			
2a. SECURITY CLASSIFICATION AUTHORITY		3. DISTRIBUTION/AVAILABILITY OF REPORT Approved for public release; distribution unlimited.			
2b. DECLASSIFICATION/DOWNGRADING SCHEDULE					
4. PERFORMING ORGANIZATION REPORT NUMBER(S) AFIT/GAE/AA/85D-16		5. MONITORING ORGANIZATION REPORT NUMBER(S)			
6a. NAME OF PERFORMING ORGANIZATION SCHOOL OF ENGINEERING	6b. OFFICE SYMBOL (If applicable) AFIT/EN	7a. NAME OF MONITORING ORGANIZATION			
6c. ADDRESS (City, State and ZIP Code) Air Force Institute of Technology Wright-Patterson AFB, Ohio 45433		7b. ADDRESS (City, State and ZIP Code)			
8a. NAME OF FUNDING/SPONSORING ORGANIZATION	8b. OFFICE SYMBOL (If applicable)	9. PROCUREMENT INSTRUMENT IDENTIFICATION NUMBER			
8c. ADDRESS (City, State and ZIP Code)		10. SOURCE OF FUNDING NOS.			
		PROGRAM ELEMENT NO.	PROJECT NO.	TASK NO.	WORK UNIT NO.
11. TITLE (Include Security Classification) See Box 19					

12. PERSONAL AUTHOR(S)
Richard A. Walley, M.S., Capt.,USAF

13a. TYPE OF REPORT MS Thesis	13b. TIME COVERED FROM _____ TO _____	14. DATE OF REPORT (Yr., Mo., Day) 1985 December	15. PAGE COUNT 89

16. SUPPLEMENTARY NOTATION

17.	COSATI CODES		18. SUBJECT TERMS (Continue on reverse if necessary and identify by block number)
FIELD	GROUP	SUB. GR.	Composites, Vibrations, Holography, Finite Elements,
11	04		STAGSC-1, Natural Frequencies, Mode Shapes
20	11		

19. ABSTRACT (Continue on reverse if necessary and identify by block number)

11)   Title: NATURAL FREQUENCIES AND MODE SHAPES OF CURVED RECTANGULAR
      ~~CURVED~~ COMPOSITE PANELS WITH INTERIOR CUTOUTS   THESIS

      Thesis Advisor: Dr Ronald L. Hinrichsen

Approved for public release: IAW AFR 190-1
~~(signature)~~ 16 AUG 86
LYNN E. WOLAVER
Dean for Research and Professional Development
Air Force Institute of Technology (ATC)
Wright-Patterson AFB OH 45433

20. DISTRIBUTION/AVAILABILITY OF ABSTRACT UNCLASSIFIED/UNLIMITED ☒ SAME AS RPT. ☐ DTIC USERS ☐	21. ABSTRACT SECURITY CLASSIFICATION UNCLASSIFIED	
22a. NAME OF RESPONSIBLE INDIVIDUAL Dr. Ronald L. Hinrichsen	22b. TELEPHONE NUMBER (Include Area Code) (513) 255-3069	22c. OFFICE SYMBOL AFIT/EN

DD FORM 1473, 83 APR   EDITION OF 1 JAN 73 IS OBSOLETE.   UNCLASSIFED

UNCLASSIFIED
SECURITY CLASSIFICATION OF THIS PAGE

> A finite element computer code, STAGSC-1 and holographic interferometry were used to determine the effects of interior cutouts (2 x 2, 2 x 4, and 4 x 4 inch) on the first five natural frequencies and mode shapes of curved Graphite Epoxy panels. The panels are a quasi-isotropic layup {0, -45, 45, 90}$_s$ with a 12 inch chord and height. Both the finite element and holographic analysis were conducted using clamped-clamped boundary conditions.

The vibration branch of STAGSC-1 is a energy technique based on small displacements and linear elastic stress-strain relationships. When compared with the time averaged holograms of the experimentally determined natural frequencies and mode shapes, the two techniques show a close correlation of both frequency and shape.

It was found that for the 2 x 2 inch cutout, the mode shapes change very little while the natural frequencies displayed a small decrease for the higher modes. The 2 x 4 inch cutout retained the general mode shape of the solid panel for the first two modes. The third through the fifth mode shapes were changed by this cutout and the loss of panel stiffness was visible. The 4 x 4 inch cutout exhibit both a switch in switch in symmetry of the first two modes and a general decrease in natural frequencies. (Theses).

UNCLASSIFIED

END

FILMED

4-86

DTIC